Dynamics of moving cavity solitons in two-level laser system from symmetric gaussian input: vectorial cubic-quintic complex Ginzburg–Landau equation

Alain Djazet[1,3] · Serge I. Fewo[1] · Conrad B. Tabi[2] · Timoléon C. Kofané[1,2,3]

Abstract

This paper studies the interaction of an electromagnetic field with the matter in a laser cavity without assuming a fixed direction of the transverse electric field, described by the two-level Maxwell–Bloch equations. The derivation of the laser (3+1)-dimensional vectorial cubic-quintic complex Ginzburg–Landau equation is reported using a perturbative nonlinear analysis performed near the laser threshold. Considering the vector (2+1)D cubic-quintic complex Ginzburg–Landau equation, the stability of the moving dissipative solitons in the laser cavity is analyzed. Using the variational approximation, stability conditions and propagation trajectories of dissipative solitons are derived. Direct numerical simulations fully confirm analytical predictions of dissipative solitons trapped in an effective potential well. Potential applications of the obtained results related to spatial dissipative solitons, may be found in class B laser by considering solitons as individual addressable and shift registers of the all-optical data processing systems.

1 Introduction

New theoretical approaches, experimental analyses, and systematic use of computer science in data processing have been developed during the past 20 years in several types of lasers, which are very complex devices, having rich temporal, spatial, and spatiotemporal dynamics [1]. These different types of lasers can be classified into [2] Class A (for example, dye lasers) [3, 4], Class B (semiconductor lasers, CO_2 lasers,

✉ Alain Djazet
djazet.alain@yahoo.fr

Serge I. Fewo
sergefewo@yahoo.fr

Conrad B. Tabi
conrad@aims.ac.za; tabic@biust.ac.bw

Timoléon C. Kofané
tckofane@yahoo.com

[1] Laboratoire de Mécanique, Département de Physique, Faculté des Sciences, Université de Yaoundé I, B.P. 812, Yaoundé, Cameroun

[2] Botswana International University of Science and Technology, Private Bag 16, Palapye, Botswana

[3] Centre d'Excellence Africain en Technologies de l'Information et de la Communication (CETIC), University of Yaounde I, Yaoundé, Cameroon

and solid-state lasers) [5, 6], and Class C (the only example being the far-infrared lasers) [7], depending on the decay rate of the photons, the carriers, and the material polarization. However, this classification does not apply to inhomogeneously broadened lasers, including He-Ne, argon-ion, and Xe. Different dynamical features have been described when comparing these lasers, including instabilities, cascades of bifurcations, multistability, and sudden chaotic transitions [1]. Many other fascinating features and properties concerned with chaotic dynamics have been extensively addressed in relevant semiconductor laser systems because of their potential applications in chaotic optical communications [8]. Further studies have suggested that optical cavities, also called cavity solitons, are present in many externally driven optical systems. However, their existence in laser systems is limited to the well-known laser with saturable absorbers, two-photon lasers, lasers with dense amplifying medium, or lasers pumped by squeezed vacuum [9].

Several models have been proposed to describe how spatiotemporal dynamics emerge in large-aperture lasers. For example, the two-photon lasers have been the subject of continued theoretical attention since the early days of the laser era. The theoretical interest of the two-photon laser lies in the intrinsic nonlinear nature of the two-photon interaction. The Maxwell–Bloch (MB) equations give the most successful theoretical approach. The laser is a system where

the number of photons is much larger than one, thus allowing a semi-classical treatment of the electromagnetic field inside the cavity through the Maxwell equations, which has been developed by Lamb [10] and independently by Haken [11]. The semi-classical laser theory ignores the quantum-mechanical nature of the electromagnetic field, and the amplifying medium is modeled quantum-mechanically as a collection of two-level atoms through the Bloch equations.

The linear analysis and numerical integration of the full MB equations [12] have been used to interpret the features of the experiment that cannot be fully understood with a perturbative model, such as the observed evolution from order to fully developed turbulence as the Fresnel number increases up to a critical control-parameter threshold [13]. In addition, it has been shown that the MB equations with a homogeneous line broadening are appropriate for the description of the amplification of short pulses in the multilevel atomic iodine amplifier [14]. Some prototype of nonlinear evolution equations has been constructed by singular perturbation methods, using the MB equations as the starting point, to reproduce the spatiotemporal dynamics of the large-aperture lasers.

The first class of prototype equations which describe, for example, the class-A laser-pattern dynamics, such as the multi-transverse-mode lasers, is the cubic complex Ginzburg–Landau (CGL) equation. The existence of a vortex solution of the laser equations, the stability of symmetric vortex lattices in the laser beams, the transition to nonsymmetric patterns dominated by titled waves, and disordered spatial distribution have been well-reproduced by the cubic CGL equation [15–19]. To prevent the "blowup" of the solutions of the cubic CGL equation for negative detuning, the cubic CGL equation, which possesses fourth- and higher-order diffusion terms and which describes the excitation of transverse modes and structure formation in a laser correctly, has been derived [20]. It should also be mentioned that the adiabatic elimination of irrelevant variables has been shown to be very sensitive to the method used for the perturbation expansions in the case of partial differential equations which describe laser dynamics. That is why the center manifold theorem for eliminating irrelevant variables has been used, leading to the cubic CGL equation in the small-field limit. The particular feature of the center manifold theory is that it is a solid mathematical framework within which the fast variables, as well as the characteristic scaling of the long-term dynamics, are properly determined [21]. It has also been shown that the cubic-quintic CGL equation is a continuous approximation to the dynamics of the field in a passively mode-locked laser [22].

The second class of prototype equations, which provides the generic description of transverse pattern formation in wide aperture, single longitudinal mode, two-level lasers, when the laser is operating near peak gain, is the complex Swift–Hohenberg equation for class A and C lasers [23]. Indeed, the complex Swift–Hohenberg equation comes naturally as a solvability condition for the existence of solutions to the MB laser equations in the form of asymptotic series in powers of the small detuning parameter [23]. In addition, when the laser pattern dynamics is sensitive to the degree of stiffness of the original physical problem, such as in the class-B lasers, the amplitude equations are the complex Swift–Hohenberg equation coupled to a mean flow [23], which is consistent with the observation that the population inversion variable in the MB laser equations acts as a weakly damped mode. Otherwise, the Swift–Hohenberg equation has been considered for a passive optical cavity driven by a coherent external field, valid close to the onset of optical bistability [24]. Moreover, theoretical studies of spatiotemporal structures of lasers with a large Fresnel number of the laser cavity have been successfully described in the cases in which two coupled fields are involved in the dynamics for class-B lasers. For example, it has been shown that two generic instabilities may destabilize the homogeneous steady-state solution. The first is a long-wavelength instability related to the electromagnetic field's phase invariance and is described by a scalar field obeying the Kuramoto-Shivasinsky equation. The second is a short wavelength instability which corresponds to a Hopf bifurcation and is characterized by a complex field that follows a Swift–Hohenberg equation.

The third class of prototype equations, which contains a phenomenological aspect and whose use in the theoretical description of the pulse dynamics in a mode-locked laser, was pioneered by Haus and Mecozzi [25]. Assuming that only one polarization state plays a role and that the change of the pulse per round trip is small, so that one can replace the discrete laser components with continuous approximations, Haus and Mecozzi [25] obtained a master equation which is nothing but the stationary version of the cubic CGL equation. The coefficients that appear in the model were related to the physical parameters in a rather phenomenological way [25, 26].

All these three classes of prototype equations are scalar since it is usually considered that the polarization degree of freedom of the electromagnetic field is fixed either by material anisotropies or by experimental arrangement. Thus, the description of the dynamics is done in terms of a scalar field. It has been shown that the cavity-synchronous phase or amplitude modulation technique transforms passively mode-locked optical oscillators into actively mode-locked lasers [27]. Mixing passive and active mode-locking in the same device results in a new class of optical oscillators generating short pulses. To model this laser system, as an example, the scalar cubic-quintic CGL equation has been used with terms corresponding to active mode-locking in addition to the usual passive mode-locking terms [28]. However, the inclusion of a quintic saturating term in the scalar cubic-quintic CGL equation was shown to be essential for the stability of pulsed solutions [29]. Since the scalar cubic-quintic CGL equation is non-integrable, which means that general analytical solutions are unavailable,

selected analytical solutions can only be found for specific relations between the equation parameters. More complicated solutions for the cubic-quintic CGL equations, such as pulsating, creeping, or exploding solutions, have been reported numerically [30]. It is also well known that laser systems are made of several components; an accurate model should then involve consecutive sets of propagation equations. Models can be vectorial when the polarization nature of light is involved, including the delayed response of the saturable absorber and gain medium. The possibility of vectorial topological defects which are not predictable by the scalar theory was first analyzed by Gil [31]. Using standard perturbative nonlinear analysis, performed near the laser threshold, Gil derived a (3+1)-dimensional ((3+1)D) vectorial cubic CGL equation when considering the interaction of an electromagnetic field with the matter in a laser cavity without the assumption of a fixed direction of the transverse electric field. Different kinds of pattern formation are present in the dynamic states of the one-spatial dimension (localized structures) [32] and of the two-spatial dimensions (topological defects) [33–36] for the vectorial cubic CGL equation. Examples are the synchronization properties of spatiotemporally chaotic states [33], the identification of a transition from a glass to a gas phase [34], and the formation and annihilation processes leading to different types of defects [35]. In addition, creation and annihilation processes of different kinds of vector defects, as well as a transition between different regimes of spatiotemporal dynamics, have been described [36]. Although many models have been derived from describing the dynamics of the solitons cavity, vector cubic-quintic CGL models have not been addressed yet in the case of cavity solitons. We demonstrate that many cavity solitons species can be obtained due to the physical processes such as third-harmonic generation, the contribution of one-photon resonant, and the two-photon-resonant.

The present work aims to understand the physical processes involved in spatial pattern formation from a two-level atomic system controlled by an intense laser field. The approach taken here parallels that of Gil [31] for the vectorial cubic CGL equation. We start with the Maxwell–Bloch equations describing the propagation of a slowly varying field envelope through a collection of two-level atoms when the interaction of an electromagnetic field with the matter in a laser cavity is considered, without the assumption of a fixed direction of the transverse electric field. Then, we report on the derivation of the laser (3+1)D vectorial cubic-quintic CGL equation. Furthermore, based on the variational approach, we discuss, theoretically and numerically, the dynamical properties of the moving vector dissipative solitons for several dynamical regimes of the coupled cubic-quintic complex Ginzburg–Landau (CQCGL) equation [37]. The problem of multidimensional soliton instabilities leads to the collapse and depends on the number of space dimensions and strength of nonlinearity [38]. It has been demonstrated that to create the stable dissipative solitons of scalar CQCGL equation, the phenomenon of wave collapse (catastrophic self-focusing) must be controlled [37–40]. In some recent theoretical and experimental studies, generic approaches for the realization of stabilized multidimensional fundamental and vortex solitons are based on the use of trapping potentials created by shallow modulations of the refractive index of the material in the transverse plane, and the materials with saturable or competing nonlinearities [41–43]. This is observed in diverse physical contexts such as matter- wave condensates and ultradilute quantum liquids, liquid crystals and ferrofluids, nonlinear optics and ultrashort few-cycle optical pulses. To understand the achievement of the complex configuration of the moving of stable multidimensional dissipative solitons of coupled CQCGL equations, the stability approach is performed based on the soliton trapped at the bottom of the effective potential well [38, 44].

This paper is organized as follows: In Sect. 2, we derive the laser (3+1)D vector CQCGL equation which describes the laser pattern dynamics. Section 3 presents the dynamical equations describing the solution parameters, followed by the research of analytical stationary solutions. Section 4 is devoted to deriving the effective potential associated with the particle-like dynamic of the dissipative solitons, along with numerical results. Section 5 presents some concluding remarks.

2 Derivation of the laser (3+1)D vector cubic-quintic CGL equation

We consider the behavior of a slowly varying field envelope through a collection of two-level atoms with a transition frequency w_a between the lasing levels and relaxation rates $\gamma_\perp$ and $\gamma_\parallel$ for the polarization and the population inversion, respectively. During the interaction of an electromagnetic field with the matter, the assumption of a fixed direction of the transverse electric field is ignored in a laser cavity. The basic equations of motion are the well-known MB equations [31, 45] written as

$$\frac{\partial^2 \mathbf{E}}{\partial t^2} = -\mu_0 c^2 \frac{\partial^2 \mathbf{P}}{\partial t^2} + c^2 \left[\nabla^2 \mathbf{E} - \nabla(\nabla.\mathbf{E})\right] - \kappa \frac{\partial \mathbf{E}}{\partial t}, \quad (1a)$$

$$\frac{\partial^2 \mathbf{P}}{\partial t^2} = -\gamma_\perp \frac{\partial \mathbf{P}}{\partial t} - w_a^2 \mathbf{P} - gD\mathbf{E}, \quad (1b)$$

$$\frac{\partial D}{\partial t} = -\gamma_\parallel \left(D - D_0\right) + \frac{2}{\hbar w}\left(\mathbf{E}.\frac{\partial \mathbf{P}}{\partial \mathbf{t}}\right), \quad (1c)$$

where $\nabla = \frac{\partial}{\partial x}\mathbf{i} + \frac{\partial}{\partial y}\mathbf{j} + \frac{\partial}{\partial z}\mathbf{k}$ and $\nabla^2 = \frac{\partial^2}{\partial x^2} + \frac{\partial^2}{\partial y^2} + \frac{\partial^2}{\partial z^2}$, with $\mathbf{i}$, $\mathbf{j}$ and $\mathbf{k}$ the spatial directions, for the envelope of the electric field $\mathbf{E}$, the envelope variable of the atomic polarization $\mathbf{P}$, and the population inversion D, respectively. The parameter

μ_0 is the magnetic susceptibility, c is the speed of light, κ is the cavity damping coefficient and $\hbar$ is Planck's constant. Assuming that the electric field frequency w is very close to the atomic frequency w_a, it follows that $\hbar w$ is the energy gap between the two atomic levels, g is the coupling constant between the electric field and the population inversion, and D_0 is the pumping term [31]. It is well known that the atomic polarization of the two-level atoms can be expanded as

$$\mathbf{P} = \epsilon \mathbf{P_1} + \epsilon^2 \mathbf{P_2} + \epsilon^3 \mathbf{P_3}, \tag{2}$$

where ϵ is a small parameter. In the following, we assume the electric field $\mathbf{E}$ to be taken as $\mathbf{E} = \epsilon \mathbf{E_1}$, which restricts the problem to the case of a single harmonic. Assuming also that $\mathbf{E_1} = \mathbf{E_1^1}$, we obtain

$$\mathbf{P_1} = \mathbf{P_1^1}, \quad \mathbf{P_2} = \mathbf{P_2^1}, \quad \mathbf{P_3} = \mathbf{P_3^1} + \mathbf{P_3^3}, \tag{3}$$

with

$$\mathbf{P_1^1} = \frac{1}{\mu_0 c^2}\left(-1 + \frac{ik}{w_a}\right)\mathbf{E_1^1}, \quad \mathbf{P_2^1} = \frac{ig}{\gamma_\perp w_a}\left(D_1^0 \mathbf{E_1^1}\right),$$

$$\mathbf{P_3^1} = \frac{ig}{\gamma_\perp w_a}\left(D_2^0 \mathbf{E_1^1} + D_2^2 \mathbf{E_1^{-1}}\right), \tag{4}$$

$$\mathbf{P_3^3} = \frac{ig}{\left(8w_a - 3i\gamma_\perp\right)}\left(D_2^2 \mathbf{E_1^1}\right),$$

and

$$D_1^0 = D_0, \quad D_2^0 = \frac{2i}{\hbar \gamma_\parallel}\left(\mathbf{P_1^1}\mathbf{E_1^{-1}} - \mathbf{P_1^{-1}}\mathbf{E_1^1}\right),$$

$$D_2^2 = \frac{2i}{\hbar\left(\gamma_\parallel + 2iw_a\right)}\left(\mathbf{P_1^1}\mathbf{E_1^1}\right).$$

Appendix A gives more details. We see that the nonlinear polarization $\mathbf{P_3} = \upsilon(\mathbf{E}.\mathbf{E}^*)\mathbf{E} + \varrho(\mathbf{E}.\mathbf{E})\mathbf{E}^* + \varsigma(\mathbf{E}.\mathbf{E})\mathbf{E}$ consists of tree contributions. Parameters υ, ϱ, and ς depend on the laser parameters. This form of the nonlinear polarization corresponds to materials possessing a higher degree of spatial symmetry (isotropic material) [46]. These contributions have very different physical characters. In terms of the energy level diagram, the first contribution with parameter υ has the vector of nature $\mathbf{E}$ and illustrates one-photon-resonant contribution to the nonlinear coupling. The second contribution with parameter ϱ has the vector nature of $\mathbf{E}^*$ and illustrates two-photon-resonant processes, produces a nonlinear polarization with the opposite handedness. The third contribution with parameter ς illustrates the process of third-harmonic generation. For the case of third-harmonic generation, three physical processes to enhance the efficiency of the third-harmonic generation through the technique of resonance enhancement are illustrated: (a) the one-photon transition is nearly resonant, (b) the two-photon transition is nearly resonant, and (c) the three-photon transition is nearly resonant. However, the method of (b) is usually the preferred way in which to generate the third-harmonic field with high efficiency, for the following reason: For the case of a one-photon resonance (a), the incident field experiences linear absorption is rapidly attenuated as it propagates through the medium. Similarly, for the case of the three-photon resonance (c), the generated field experiences linear absorption. However, for the case of a two-photon resonance (b), there is no linear absorption to limit the efficiency of the process. These predictions are exceptionally reliable for the case of atomic vapors because the atomic parameters (such as atomic energy levels and dipole transition moments) that appear in the quantum-mechanical expressions are often known with high accuracy. In addition, since the energy levels of free atoms are very sharp (as opposed to the case of most solids, where allowed energies have the form of broad bands), it is possible to obtain very large values of the nonlinear polarization through the technique of resonance enhancement [46].

We also assume that the traveling waves are lasing with frequency ω_a and critical vector $k_c = \pm\omega_a/c$. In addition, the longitudinal direction $\mathbf{z}$ is selected by the geometry of the laser medium or the mirrors. The direction of propagation is given by $\mathbf{K_c} = k_c\mathbf{z}$, though a priori both directions of propagation are equiprobable. Once the atomic polarizability is known, the well-established perturbative nonlinear analysis is performed near the laser threshold by introducing a small parameter ($\epsilon << 1$) so that [31]

$$D_0 = D_{OC} + \epsilon^2 \widetilde{D}_0, \tag{5}$$

where D_{OC} is a critical value given by $D_{OC} = \frac{\kappa\gamma_\perp}{\mu_0 c^2 g}$. The laser variables will also depend on two slow spatial and temporal scales, respectively,

$$\xi = \epsilon x, \quad \zeta = \epsilon y, \tag{6a}$$

and

$$Z = \epsilon^2 z, \quad \tau = \epsilon^2 t. \tag{6b}$$

Then, close enough to the laser threshold, we look for solutions ($\mathbf{E}$, $\mathbf{P}$, D) of Eq. (1) in the form of a power series expansion in the small parameter ϵ as follows:

$$\begin{pmatrix} \mathbf{E} \\ \partial_t\mathbf{E} \\ \mathbf{P} \\ \partial_t\mathbf{P} \\ D \end{pmatrix} = \begin{pmatrix} 0 \\ 0 \\ 0 \\ 0 \\ D_0 \end{pmatrix} + \epsilon \begin{pmatrix} \mathbf{E}_1 \\ \partial_t\mathbf{E}_1 \\ \mathbf{P}_1 \\ \partial_t\mathbf{P}_1 \\ D_1 \end{pmatrix} + \epsilon^2 \begin{pmatrix} \mathbf{E}_2 \\ \partial_t\mathbf{E}_2 \\ \mathbf{P}_2 \\ \partial_t\mathbf{P}_2 \\ D_2 \end{pmatrix} + \cdots, \tag{7}$$

with

$$\begin{pmatrix} \mathbf{E}_1 \\ \partial_t \mathbf{E}_1 \\ \mathbf{P}_1 \\ \partial_t \mathbf{P}_1 \\ D_1 \end{pmatrix} = \begin{pmatrix} \mathbf{A} \\ i w_a \mathbf{A} \\ \frac{1}{\mu_0 c^2}(-1 + \frac{ik}{w_a})\mathbf{A} \\ \frac{i w_a}{\mu_0 c^2}(-1 + \frac{ik}{w_a})\mathbf{A} \\ 0 \end{pmatrix} e^{i(wt - k_c z)} + c.c., \tag{8}$$

with $\mathbf{A} \perp \mathbf{Z}$, where $\mathbf{A}$ is slowly varying field amplitude in space and time. After inserting Eqs. (5)–(7) into the MB equations, rearranging terms and making use of Eqs. (3), (2) and (8), and identifying the coefficients of powers ϵ at each order, we obtain, by applying the solvability conditions at $0(\epsilon^2)$ and $0(\epsilon^3)$, the laser $(3 + 1)D$ vectorial CQCGL equation [47]

$$\begin{aligned} \frac{\partial \mathbf{A}}{\partial \tau} &= z_1 \mathbf{A} - z_2 \left(\frac{\partial}{\partial \mathbf{Z}} + \frac{i}{2k_c} \nabla_\perp^2 \right) \mathbf{A} \\ &\quad + z_3 \left(\frac{\partial}{\partial Z} + \frac{i}{2k_c} \nabla_\perp^2 \right)^2 \mathbf{A} - z_4 (\mathbf{A} \cdot \mathbf{A}^*) \mathbf{A} \\ &\quad - z_5 (\mathbf{A} \cdot \mathbf{A}) \mathbf{A}^* + z_6 (\mathbf{A}^2 \cdot \mathbf{A}^{*2}) \mathbf{A} \\ &\quad + z_7 (\mathbf{A}^3 \cdot \mathbf{A}^*) \mathbf{A}^*, \end{aligned} \tag{9}$$

where $\nabla_\perp^2 = \frac{\partial^2}{\partial \xi^2} + \frac{\partial^2}{\partial \zeta^2}$ represents a two-dimensional Laplacian operator and the asterisk $(*)$ stands for the complex conjugate, while the coefficients $z_i(i = 1, 2, \dots, 7)$ are given in the Appendix. Equation (9) describes the behavior of the electric field in the medium. When coefficients $z_6 = z_7 = 0$, in Eq. (9), we recover the laser $(3 + 1)D$ vectorial CCGL equation that was introduced early by Gil [31] as a vector order parameter for an unpolarized laser and its vectorial topological defects. As can be seen, the model Eq. (9) has never been derived previously for the best of our knowledge. The coefficients z_6 and z_7 are simultaneously lead to the contribution of nonlinear polarization with parameter υ that has the vector nature of $\mathbf{E}$, the nonlinear polarization with parameter ϱ that has the vector nature of $\mathbf{E}^*$, and the contribution of the nonlinear polarization with parameter ς that illustrates the process of third-harmonic generation.

Due to the highly nonlinear nature of Eq. (9), we introduce a number of useful simplifications: (i) we use the traditional uniform field limit which requires that both the mirror transmittivity and the gain per pass of the active medium be small, while their ratio may be arbitrary but finite; (ii) a large free spectral range; (iii) the number of modes that are significantly excited is manageably small [48]; (iv) the fourth-order derivative is neglected [31]. In this way, the new field amplitude obeys the equation of motion

$$\mathbf{A} = \mathbf{B}(\xi, \zeta, \tau) \exp(-i\Delta Z), \tag{10}$$

with Δ being the wave vector, and the amplitude $\mathbf{B}(\xi, \zeta, \tau)$ is governed by the equation

$$\begin{aligned} \frac{\partial \mathbf{B}}{\partial \tau} &= c_1 \mathbf{B} + c_2 \nabla^2 \mathbf{B} - c_3 (\mathbf{B}.\mathbf{B}^*) \mathbf{B} - c_4 (\mathbf{B}.\mathbf{B}) \mathbf{B}^* \\ &\quad + c_5 (\mathbf{B}^2 . \mathbf{B}^{*2}) \mathbf{B} + c_6 (\mathbf{B}^3 . \mathbf{B}^*) \mathbf{B}^*, \end{aligned} \tag{11}$$

where $c_1 = z_1 + \Delta(-\Delta z_3 + i z_2)$, $c_2 = \frac{(2\Delta z_3 - i z_2)}{2k_c}$, $c_3 = z_4$; $c_4 = z_5$, $c_5 = z_6$, $c_6 = z_7$, with $\mathbf{B} \perp \mathbf{Z}$. We consider the case where $\mathbf{B}$ has two complex components such as $\mathbf{B} = (B_\xi, B_\zeta)$, describing the complex slowly varying amplitudes of the electric field [49]. The right and left circularly polarized components (B_+, B_-) are related to the cartesian components by the formulas $B_\xi = (B_+ + B_-)/\sqrt{2}$ and $B_\zeta = (B_+ - B_-)/i\sqrt{2}$ [46]. We then obtain the coupled equations describing the dynamics of the circular components after usual scaling transformations [47, 50]

$$\begin{aligned} i\frac{\partial \psi_+}{\partial t} &+ \psi_+ + \Delta\psi_+ + |\psi_+|^2 \psi_+ + \gamma_r |\psi_-|^2 \psi_+ + \nu |\psi_+|^4 \psi_+ \\ &+ \delta_r \left(|\psi_-|^2 + 2|\psi_+|^2 \right) |\psi_-|^2 \psi_+ \\ &= i\left[\delta\psi_+ + \beta\Delta\psi_+ + \varepsilon |\psi_+|^2 \psi_+ + \mu |\psi_+|^4 \psi_+ \right. \\ &\quad \left. + \delta_i \left(|\psi_-|^2 + 2|\psi_+|^2 \right) |\psi_-|^2 \psi_+ \right], \end{aligned} \tag{12a}$$

$$\begin{aligned} i\frac{\partial \psi_-}{\partial t} &+ \psi_- + \Delta\psi_- + |\psi_-|^2 \psi_- + \gamma_r |\psi_+|^2 \psi_- \\ &+ \nu |\psi_-|^4 \psi_- + \delta_r \left(|\psi_+|^2 + 2|\psi_-|^2 \right) |\psi_+|^2 \psi_- \\ &= i\left[\delta\psi_- + \beta\Delta\psi_- + \varepsilon |\psi_-|^2 \psi_- + \mu |\psi_-|^4 \psi_- \right. \\ &\quad \left. + \delta_i \left(|\psi_+|^2 + 2|\psi_-|^2 \right) |\psi_+|^2 \psi_- \right], \end{aligned} \tag{12b}$$

where

$$\begin{aligned} \delta &= -c_{1i}/c_{1r}, \quad \beta = c_{2i}/c_{2r}, \quad \varepsilon = c_{3i}/c_{3r}, \\ \mu &= c_{5i}/c_{5r}, \quad \gamma_r = (c_{3r} + 2c_{4r})/c_{3r}, \\ \gamma_i &= (c_{3i} + 2c_{4i})/c_{3r}, \\ \delta_r &= -(c_{5r} + 3c_{6r})/2c_{5r}, \\ \delta_i &= -(c_{5i} + 3c_{6i})/2c_{5r}, \end{aligned} \tag{13}$$

with $\nu = sign(c_{5r}/c_{3r}^2), t \to \tau, (x, y) \to \sqrt{c_{2r}}(\xi, \zeta), \psi_\pm \to B_\pm/\sqrt{c_{3r}}$. In Eq. (12), $\nabla^2 \psi_+$ and $\nabla^2 \psi_-$ represent two-dimensional Laplacian operators describing diffraction in the transverse (x, y)-plane, $|\psi_+|^2 \psi_+$ and $|\psi_-|^2 \psi_-$ denote the cubic self-phase modulation (SPM), $|\psi_-|^2 \psi_+$ and $|\psi_+|^2 \psi_-$ correspond to the cubic cross-phase modulation (XPM), $|\psi_+|^4 \psi_+$ and $|\psi_-|^4 \psi_-$ denote the quintic SPM, $|\psi_-|^2 |\psi_+|^2 \psi_+$ and $|\psi_+|^2 |\psi_-|^2 \psi_-$ represent the mixed quintic XPM, and $|\psi_-|^4 \psi_+$ and $|\psi_+|^4 \psi_-$ denotes the quintic XPM. In the following, $\varepsilon, \mu, \gamma_r, \gamma_i, \delta_r$, and δ_i are real parameters of SPM and XPM terms of Eqs. (12). δ is related to the linear loss ($\delta < 0$) or gain ($\delta > 0$). β denotes the strength of diffraction, and ε to the nonlinear frequency detuning. μ stands for the saturation of the nonlinear

frequency detuning, γ_r and γ_i are the nonlinear cross coefficients related to the cubic XPM, δ_r and δ_i are the nonlinear cross coefficients describing the quintic XPM, ν represents the nonlinear coefficient for the quintic SPM.

3 Analytical treatment using variational approach

To remind, a study of the (2+1) D form of the CQ-CGL equation governing the evolution of the optical field in the bulk medium with the localized linear gain compensated by losses was successfully made using the variational approximation adapted to dissipative systems, in which stability domains of elliptic spinning ones, double-rotating eccentric vortices, revolving crescents, and breathers were found [51]. In addition, varieties of asymmetric rotating vortices carrying the topological charge, and four- to ten-pointed revolving stars with zero topological charge have been generated using the variational approximation [52]. To proceed with the variational method, we adopt the following appropriate notation of Eq. (12) whose the coupled CQCGL equations are rewritten as [44]:

$$
i\frac{\partial \psi_\pm}{\partial t} + \psi_\pm + \Delta\psi_\pm + |\psi_\pm|^2\psi_\pm + \gamma_r|\psi_\mp|\psi_\pm \\
+ \nu|\psi_\pm|^4\psi_\pm + \delta_r(|\psi_\mp|^2 + 2|\psi_\pm|^2)|\psi_\mp|^2\psi_\pm = iQ_\pm,
\tag{14}
$$

with

$$
Q_\pm = \delta\psi_\pm + \beta\Delta\psi_\pm + \varepsilon|\psi_\pm|^2\psi_\pm + \gamma_i|\psi_\mp|\psi_\pm \\
+ \mu|\psi_\pm|^4\psi_\pm + \delta_i(|\psi_\mp|^2 + 2|\psi_\pm|^2)|\psi_\mp|^2\psi_\pm,
\tag{15}
$$

where we have separated conservative from non-conservative terms. Solutions for such equations are assumed as a symmetric gaussians ansatz [37, 53, 54] given by

$$
\psi_\pm = A\exp\left\{ -\frac{(x \pm X_0)^2 + y^2}{2X^2} \right. \\
\left. + i[2C((x \pm X_0)^2 + y^2) \pm N(x \pm X_0) + \varphi] \right\},
\tag{16}
$$

where A is the amplitude, X is the spatial width, C is the unequal wavefront curvature, X_0 is the central position, φ is the phase and N accounts for the motion of the dissipative soliton along the transverse direction. They are all functions of the independent variable t. By means of the variational approach [38, 44, 53, 55–57], we obtain the following corresponding set of six Euler-Lagrange equations:

$$
\frac{dA}{dt} = -\frac{3}{4}A^3\varepsilon + \frac{2A^2\beta}{X^2} - \frac{5}{9}A^5\mu + 4AC + A\beta N^2 \\
- \delta A + \left(-1 + \frac{1}{2X^2} + \frac{X_0^2}{X^2}\right)A^3\gamma_i e^{-\frac{2X_0^2}{X^2}} \\
+ \left(\frac{8X_0^2}{9X^2} - 1 + \frac{1}{2X^2}\right)A^5\delta_i e^{-\frac{8X_0^2}{3X^2}},
\tag{17a}
$$

$$
\frac{dX}{dt} = -\frac{1}{4}A^2 X\varepsilon - \frac{\beta}{X} + \frac{2}{9}A^4 X\mu + 4XC(\beta CX^2 - 1) \\
+ \frac{1}{2}\left(-X + \frac{1}{X} + \frac{2X_0^2}{X}\right)A^2\gamma_i e^{-\frac{2X_0^2}{X^2}} \\
+ \left(\frac{16X_0^2}{9X} - 1 + \frac{1}{X}\right)A^4\delta_i e^{-\frac{8X_0^2}{3X^2}},
\tag{17b}
$$

$$
\frac{dC}{dt} = -\frac{1}{4X^2}A^2 - \frac{2}{9X^2}A^4\nu + \frac{4\beta C}{X^2} \\
+ \frac{\gamma_r A^2}{X^2}\left(\frac{X_0^2}{X^2} - \frac{1}{4}\right)e^{-\frac{2X_0^2}{X^2}} \\
+ \frac{2\delta_r A^4}{3X^2}\left(\frac{8X_0^2}{9X^2} - 1\right)e^{-\frac{8X_0^2}{3X^2}} \\
- \frac{1}{X^4} + 4C^2,
\tag{17c}
$$

$$
\frac{dN}{dt} = 2N\beta\left(\frac{1}{X^2} + 4X^2 C^2\right) \\
+ \left(2\gamma_i C - \frac{\gamma_r}{X^2}\right)A^2 X_0 e^{-\frac{2X_0^2}{X^2}} \\
+ \left(\delta_i C - \frac{\delta_r}{X^2}\right)\frac{16A^4 X_0}{9}e^{-\frac{8X_0^2}{3X^2}},
\tag{17d}
$$

$$
\frac{dX_0}{dt} = 2N\beta(-1 + 2X^2 C) + \gamma_i A^2 X_0 e^{-\frac{2X_0^2}{X^2}} \\
+ \frac{8\delta_i A^4 X_0}{9}e^{-\frac{8X_0^2}{3X^2}},
\tag{17e}
$$

$$
\frac{d\varphi}{dt} = 1 + 4\beta C(NX^2 - 1) + \frac{5}{9}A^4\nu + \frac{3}{4}A^2 + \frac{2}{X^2} \\
- N^2 + \left(\gamma_i NX_0 + \frac{3\gamma_r}{4} - \frac{\gamma_r X_0^2}{X^2}\right)A^2 e^{-\frac{X_0^2}{X^2}} \\
+ \frac{1}{3}\left(\frac{8\delta_i NX_0}{3} + 5\delta_r - \frac{16\delta_r X_0^2}{3X^2}\right)A^4 e^{-\frac{8X_0^2}{3X^2}}.
\tag{17f}
$$

The variational technique reveals the interaction between the symmetric Gaussian waves and the laser system during propagation, including the additional relevant effects. The dynamics of the entire soliton can be significantly affected during the propagation. However, as well as the theoretical analysis shows the influence of the system on the dissipative soliton dynamics, explicit information related to the different solutions and their stability cannot be obtained at this stage of the analytical procedure.

The steady-state solutions of the system of Eqs. (17a)–(17e) are obtained by setting the derivatives of soliton parameters with respect to *time*, to zero. Taking $X_0 = 0$, for more simplicity, and after some algebra, we obtain the following solutions that give: (i) the amplitude

$$A = \frac{3}{2}\sqrt{-\frac{1+\gamma_r}{2(\nu + 3\delta_r)}}, \tag{18}$$

(ii) the width

$$X = \left[\frac{((18\beta\delta_i + 24\delta_r) + 8(\beta\mu - \nu))A^4 + 9(\beta(\varepsilon - \gamma_i) - 1 - \gamma_r)A^2}{36(2(1+\beta^2) + \frac{\beta A^2}{2}(\gamma_i + A^2\delta_i))}\right]^{-1/2}, \tag{19}$$

(iii) the soliton velocity

$$N = \sqrt{\frac{\delta + \frac{1}{2}(\gamma_i + \varepsilon)A^2 + (\frac{\delta_i}{2} + \frac{\mu}{3})A^4}{\beta}}, \tag{20}$$

(iv) the unequal wavefront curvature

$$C = \frac{1}{2\beta X^2}, \tag{21}$$

necessary to build the steady-state solution.

4 Stability analysis and numerical results

The stability analysis of the moving dissipative soliton is performed through the effective potential [44, 58–60]. In doing so, we first investigate the possibility of the soliton trapped at the bottom of the effective potential well. The integration of the variational Eqs. (17a)–(17f) gives

$$\frac{1}{4}\left(\frac{dX}{dt}\right)^2 + U(X) = U(X_0). \tag{22}$$

The stationary solution of Eq. (22) corresponds to a particle located at the bottom of a potential well $U(X)$, whose expression is given in appendix B. In this framework, the equation that describes the dynamics of a particle in a one-dimensional potential well is

$$\frac{d^2X}{dt^2} = -2\frac{\partial U(X)}{\partial X}, \tag{23}$$

which is valid when the nonlinearity exactly balances the diffraction and the loss is exactly compensated by the gain. The graph of the effective potential shows an extremum, which is an equilibrium point. The analysis of the possibility of the soliton being trapped in the well is presented in Fig. 1. The used parameters correspond to the population inversion decay rate $\gamma_{\parallel} = 10^7 s^{-1}$, polarization decay rate $\gamma_{\perp} = 3.9 \times 10^9 s^{-1}$, the cavity loss $\kappa = 9.9 \times 10^7 s^{-1}$ and the lasing wavelength $\lambda = 10.6\ \mu m$ [61], together with the atomic transition frequency $\omega_a = 0.2 \times 10^8 s^{-1}$ for Fig. 1a, and $\omega_a = 2.5 \times 10^8 s^{-1}$ for Fig. 1b. From Fig. 1a, b, we can observe the appearance of two domains of instability (plane domain with zero potential and the domain of maximum potential), and the stability domain with minimum values of the effective potential, where the soliton can be trapped [44, 58]. The symmetric Gaussian input will be self-trapped and generate a dissipative soliton for a good choice of dissipative parameters belonging to the stable domain.
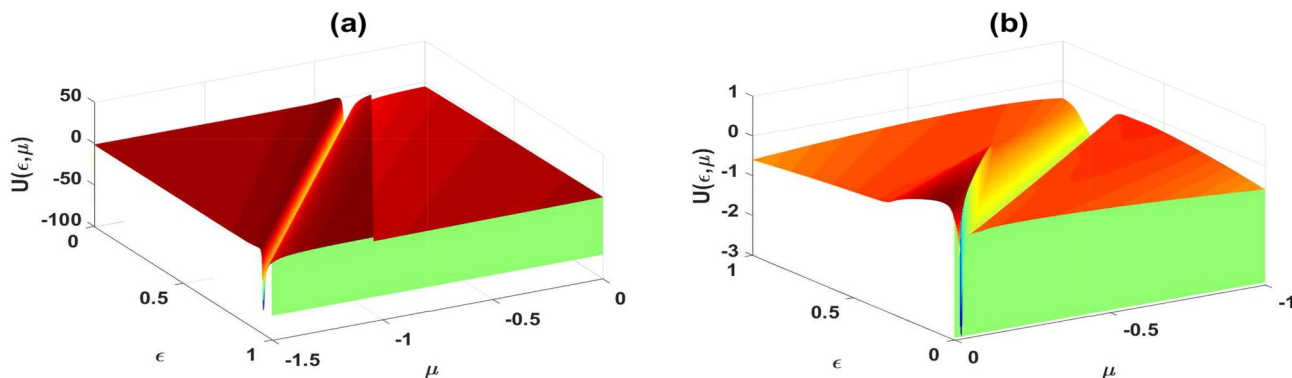

Fig. 1 Potential $U(\varepsilon, \mu)$ for the following set of parameters: $\nu = -1$, $X_0 = 12.5$; **a** $\delta = -0.159$, $\gamma_r = 1.1087$, $\gamma_i = 0.2118$, $\beta = 0.0159$, $\delta_i = 0.1289$, $\delta_r = -0.5074$, **b** $\delta = -0.13761$, $\gamma_r = 1.0535$, $\gamma_i = 0.1001$, $\beta = 0.1761$, $\delta_i = 0.43$, $\delta_r = -0.5016$

The time evolution of the solution parameters has been numerically investigated using the fourth-order Runge–Kutta computational method, which allows to integrate the system of equations obtained through the variational approach. The results that are displayed in Fig. 2a, b show that the amplitude A, the width X, the velocity N, and the unequal wavefront curvature C evolve with a slight change at the beginning of their propagation. From Fig. 2c, d (showing the input/output of the two solutions), one sees the increase of the widths, slight decrease of the intensities, and the shift of the central position corresponding to the two solutions. Despite this small difference, the variational analysis gives a detailed qualitative picture of each perturbation's role and mode of action (such as coupling, diffraction, self-phase modulation, loss, or gain) on the pulse during propagation.

To confirm our analytical predictions, we solve the coupled (2+1)D CQCGL. Equation (14) with the split-step Fourier method [44]. Using parameters corresponding to the stable domain of Fig. 1b (bottom of the effective potential), we obtain Fig. 3a, b. They present a stable evolution of the intensities of the coupled moving dissipative solitons ψ_- and ψ_+ during propagation in the space-time domain. Figure 3c, d show the corresponding spectral evolution of Fig. 3a, b. Albeit the initial shift of their central position, which is in agreement with the analytical predictions (see

Eqs. (17a)–(17f)) together with Fig. 1, solitons remain stable during propagation. However, as we have noted, a continuous shift of the initial central position during propagation, the corresponding spectral dynamics presents stable central position (see Fig. 3c, d).

Stable harmonic time evolution of solutions ψ_+ and ψ_- are shown in Fig. 4a, b. So the results are confirmed by the prediction of Haken [62], showing that the lasers are stable systems. Figure 4b, with its corresponding spectral evolution shown in Fig. 4d, reveal the moving harmonic dynamics. On the other hand, Fig. 4a and the corresponding spectral evolution (see Fig. 4c), related to the solution ψ_+, show a stationary harmonic evolution with a large period, compared to ψ_- solution. This coherent evolution is an important property of laser systems and is used in applications such as holography and interferometry [63, 64].

As a reminder, the used parameters of Fig. 4 belong to the bottom of the potential well shown in Fig. 5, obtained for $\delta_r = -0.25016$. The rest of parameters remains unchanged as in Fig. 1b.

When carefully adjusting the nonlinear parameters around the bottom of the effective potential well, a typical optical evolution of the solution is depicted and displayed in Fig 6a, b, for the maximum values of ψ_+ and ψ_-, respectively. Their corresponding spectral evolutions are given in

Fig. 2 **a**, **b** display the evolution of the amplitude, the pulse widths, the chirp, the unequal wavefront curvatures, the velocity, the central position and the phase with respect to t. **c**, **d** depict the input/output profiles of the solutions ψ_+ and ψ_- for the following set of parameters: $\delta = -0.159$, $\gamma_r = 1.1087$, $\gamma_i = 0.2118$, $\nu = -1$, $\beta = 0.0159$, $\delta_i = 0.1289$, $\delta_r = -0.5074$, and the initial central position $X_0 = 2.5$
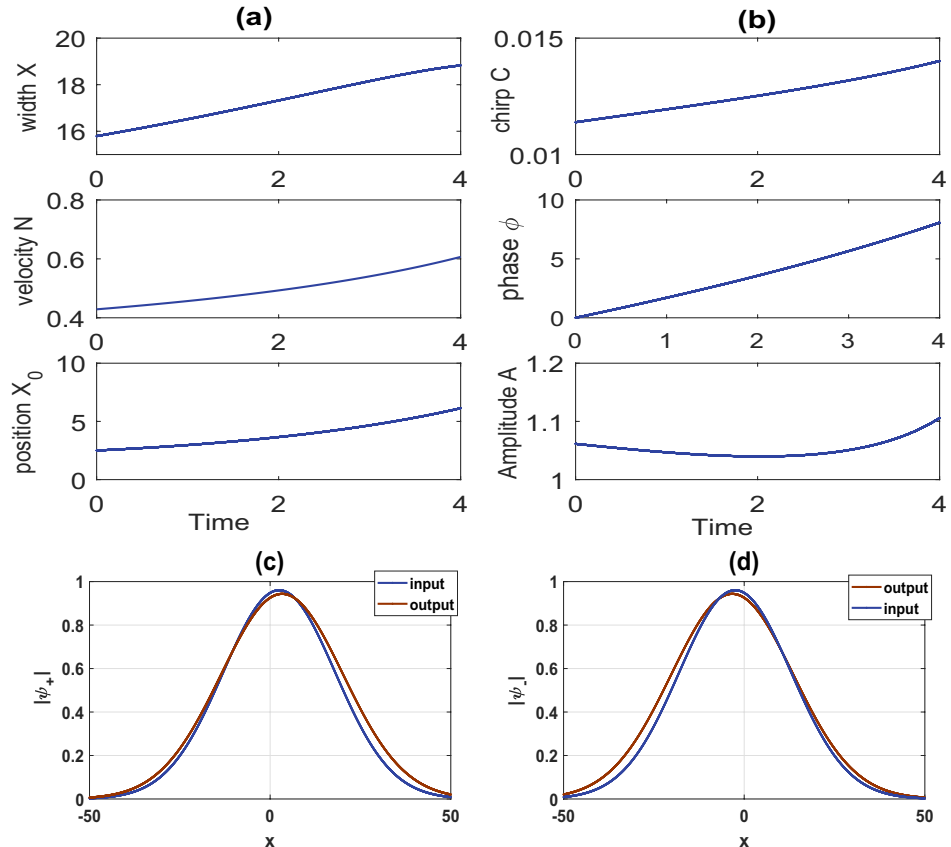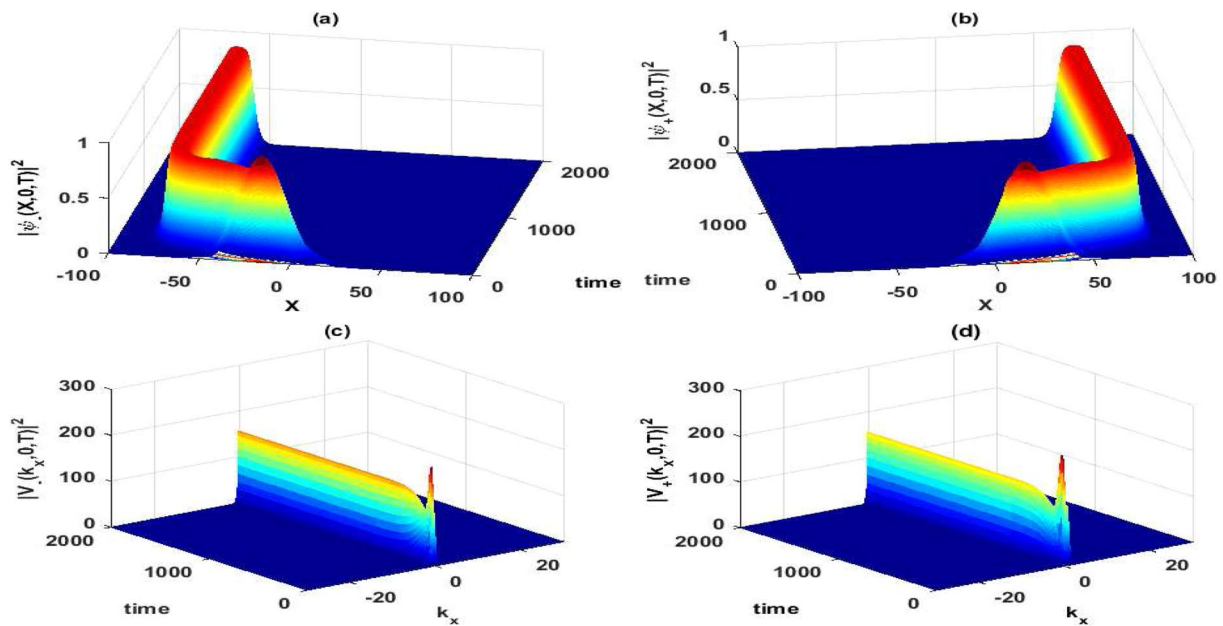
Fig. 3 a, **b** show the three dimensional spatial evolution as predicted by the stability of the dissipative soliton trapped in the potential well. **c**, **d** display their corresponding spectral evolution V_- and V_+, respectively for the values of parameters $\varepsilon = 0.72$, $\mu = -0.728$ and $X_0 = 15.5$
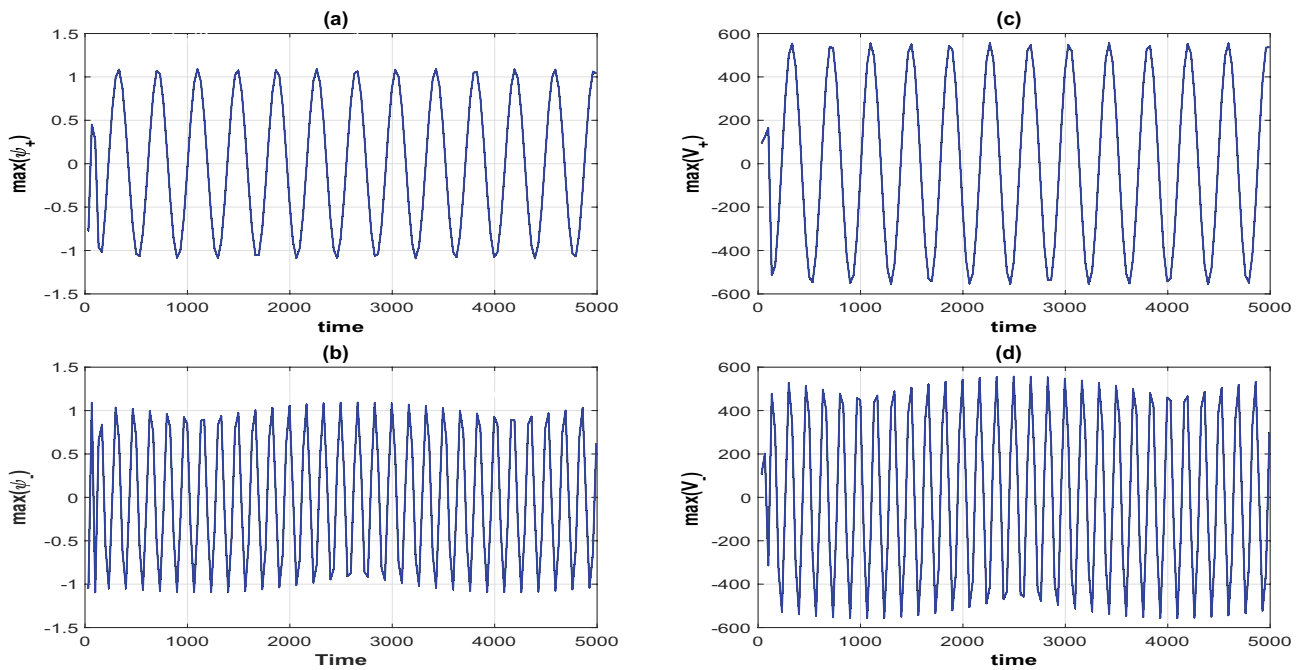

Fig. 4 a, **b** are the periodic evolution of $max(\psi_+(t))$ and $max(\psi_-(t))$ of the dissipative soliton obtained by direct numerical simulation of Eq. (13). The corresponding spectral evolution $max(V_+(t))$ and $max(V_-(t))$ are presented in **c**, **d**, with $\delta_r = -0.25016$, $\varepsilon = 0.72$, and $\mu = -0.73$, while the rest of parameters remains the same in Fig. 3

Fig. 6c, d. One should note that the comparison between Figs. 4 and 6 leads to a good agreement both for analytical and numerical results. A periodic evolution is noted in Fig. 4 using parameters taken from the bottom of the potential well. When shifting such values, we observe a gradual change in the periodicity of the solutions ψ_+ and ψ_-, which indicates a gradually lost stability as presented in Fig. 6. Interestingly, a similar result was experimentally obtained by Cohen et al. [65], using a semiconductor laser with quasi-periodic dynamics induced by external optical feedback
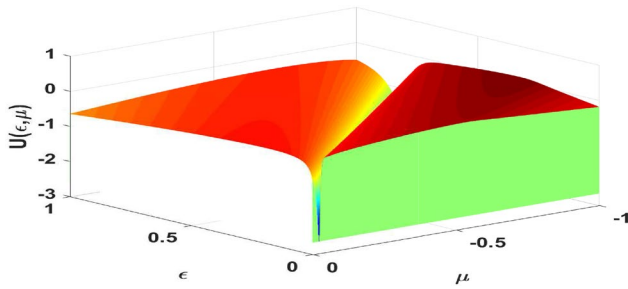
Fig. 5 Potential $U(\epsilon, \mu)$, as a function ϵ and μ, for $\delta_r = -0.25016$. The other parameters remain unchanged as in Fig. 1b

from a cavity with two arms, also known as the T-cavity. They showed the existence of frequency shifts in the spectrum occurring in the optical domain, therefore giving way for developing novel laser-feedback-based devices with the capability for subwavelength, nanoscale, multidimensional position sensing. Figure 7a, c, e for $|\psi_+(x, y)|^2$ and Fig. 7b, d, f for $|\psi_-(x, y)|^2$ present the three-dimensional evolution of the dynamics given in Fig. 4a, b, and reveal the formation of alternate structures that had been predicted and observed in the CO_2 laser [66].

Figure 8 presents profiles of dissipative solitons at different propagation times. They reveal another specificity and particularity of Eq. (14). The obtained 3D stable spatiotemporal optical solitons, by direct numerical simulations of

the proposed model equation, are among new interesting dynamical aspects of dissipative optical solitons. The results are obtained with $X_0 = 12.5$, $\delta_r = -0.3$, and the rest of the parameters are the same as those of Fig. 7.

We observe through numerical simulations that when carefully adjusting the value of δ_r, the initial symmetric solution (see Fig. 8a, b) evolves toward a new stable formation with a non-smooth vertex top profile. Recently, a similar result was obtained by Djoko et al. [55]. They showed that such profiles are stable and can be considered a potential object for long-distance transmission in communication systems. To confirm the results of Figs. 8, 9 displays the spectral evolution of the solution given in Fig. 8, and it follows that, despite the non-smooth vertex top profile, those profiles remain stable. These structures are good candidates for laser devices.

5 Conclusion

In summary, the first achievement of the present work was the successful derivation of the (3+1)D vectorial CQCGL equation, modeling the interaction of an electromagnetic field with the matter in a laser near the lasing threshold. After that, the stability of the moving dissipative solitons in the laser cavity, modeled by the coupled (2+1)D CQCGL equation, has been studied. We have derived the expression
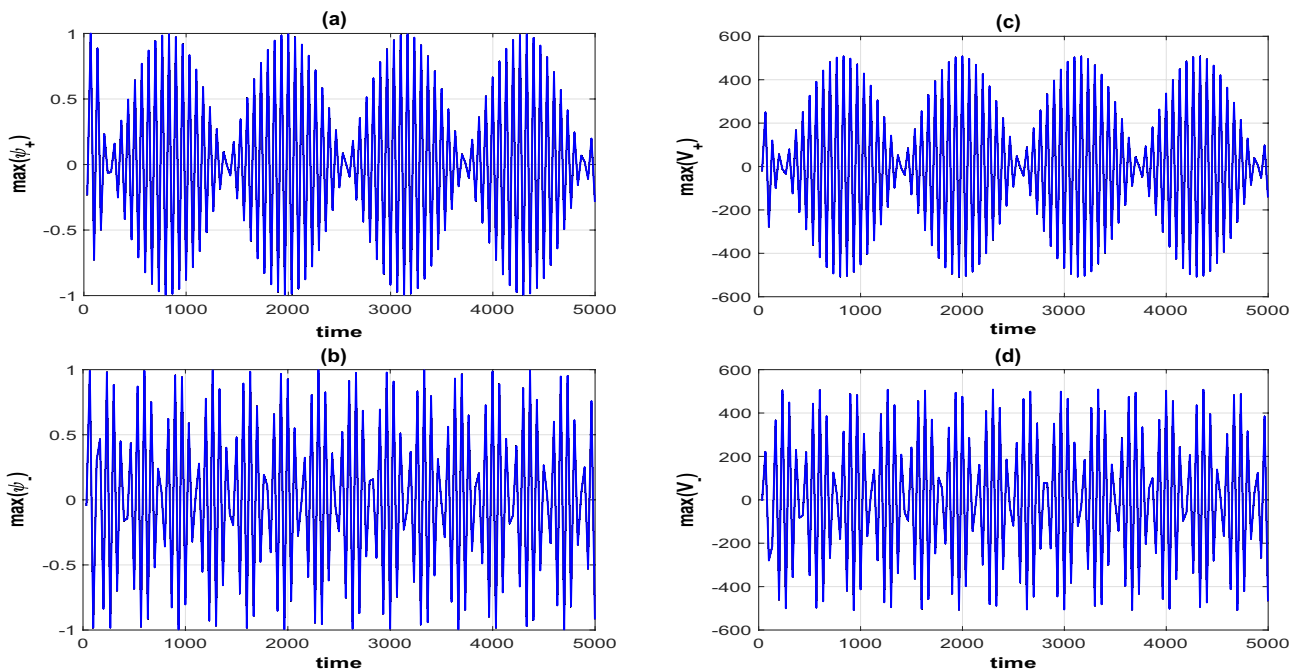

Fig. 6 a, **b** show the quasi-periodic evolution of $max(\psi_+(t))$ and $max(\psi_-(t))$ of the dissipative soliton by direct numerical simulation of Eq. (13). The corresponding spectrals evolution $max(V_+(t))$ and $max(V_-(t))$ are presented in **c**, **d**, with $\delta_r = -0.25016$, $\epsilon = 0.63051$ and $\mu = -0.728$. The rest of parameters are taken from Fig. 3
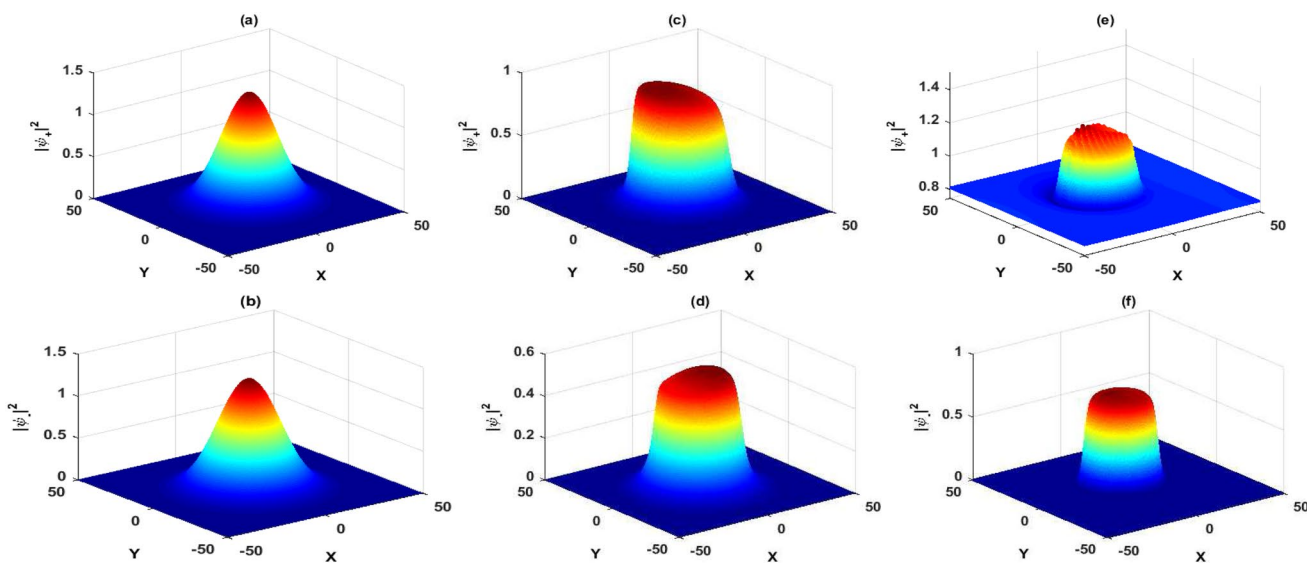
Fig. 7 Spatial profiles of the solution $\psi_+(x, y)$ (upper line) and $\psi_-(x, y)$ (bottom line) at different steps of the evolution: **a, b** $T = 0$, **c, d** $T = 4$, **e, f** $T = 10{,}000$, using the following param-eters: $\delta = -0.13761$, $\beta = 0.1761$, $\varepsilon = 0.7$, $\gamma_r = 1.0535$, $\gamma_i = 0.1001$, $\delta_i = 0.043$, $\delta_r = -0.25016$, $\nu = -1$, $\mu = -0.73$, and $X_0 = 2.5$
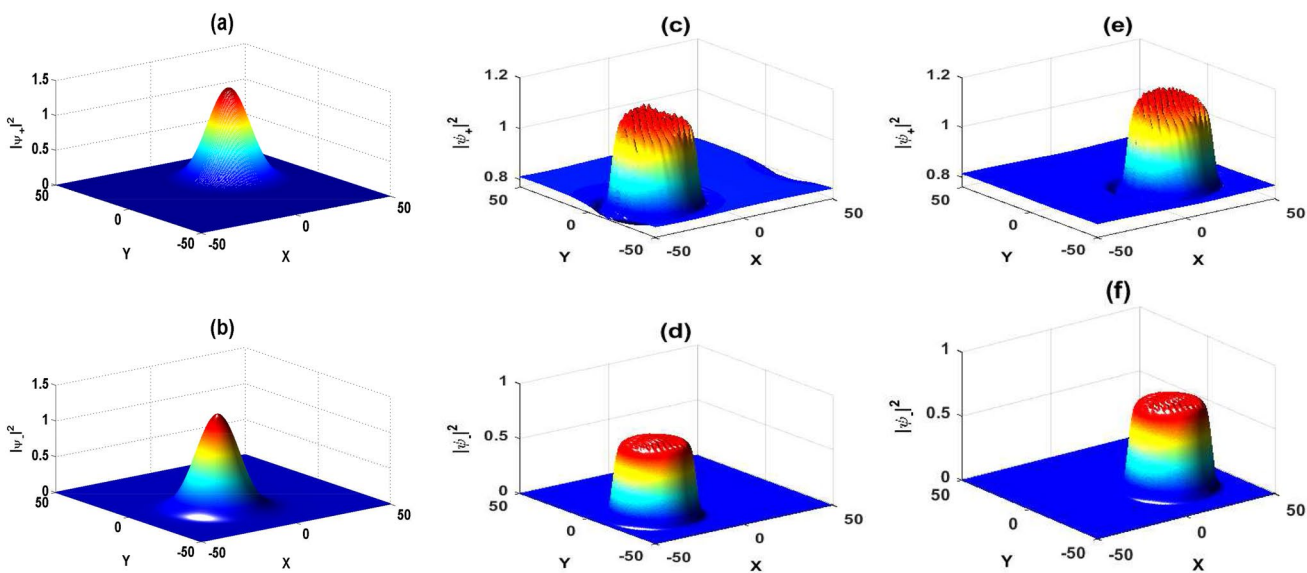

Fig. 8 Spatial profile of the solution $\psi_+(x, y)$ (upper line) and $\psi_-(x, y)$ (bottom line) at different steps of the evolution: **a, b** $T = 0$, **c, d** $T = 15{,}000$, **e, f** $T = 30{,}000$, using the following parameters val-ues: $\delta = -0.13761$, $\beta = 0.1761$, $\varepsilon = 0.7$, $\gamma_r = 1.0535$, $\gamma_i = 0.1001$, $\delta_i = 0.043$, $\delta_r = -0.3$, $\nu = -1$, $\mu = -0.73$, and $X_0 = 12.5$

of the stability condition and the propagation trajectory of solitons using the variational approach. Using the effective potential of the system, we have shown, through numerical simulations, that solitons can be trapped in the potential well, leading to a good agreement between analytical and numerical results. In such dissipative systems, cross-compensation involving self-focusing, loss/gain, and coupled effects appears to stabilize the controllable behavior of induced optical vector moving solitons during propagation.

Based on an appropriate choice of parameters, from the stability condition, we have observed a generation of harmonic to quasi-periodic patterns inherent to the laser systems. This confirms the accuracy between our analytical predictions and the long-time evolution of the expected moving dissipative solitons, as observed experimentally in the CO_2 laser.

They could be of great interest for technological applications related to laser systems to increase their efficiency. In addition, such patterns allow the development of novel
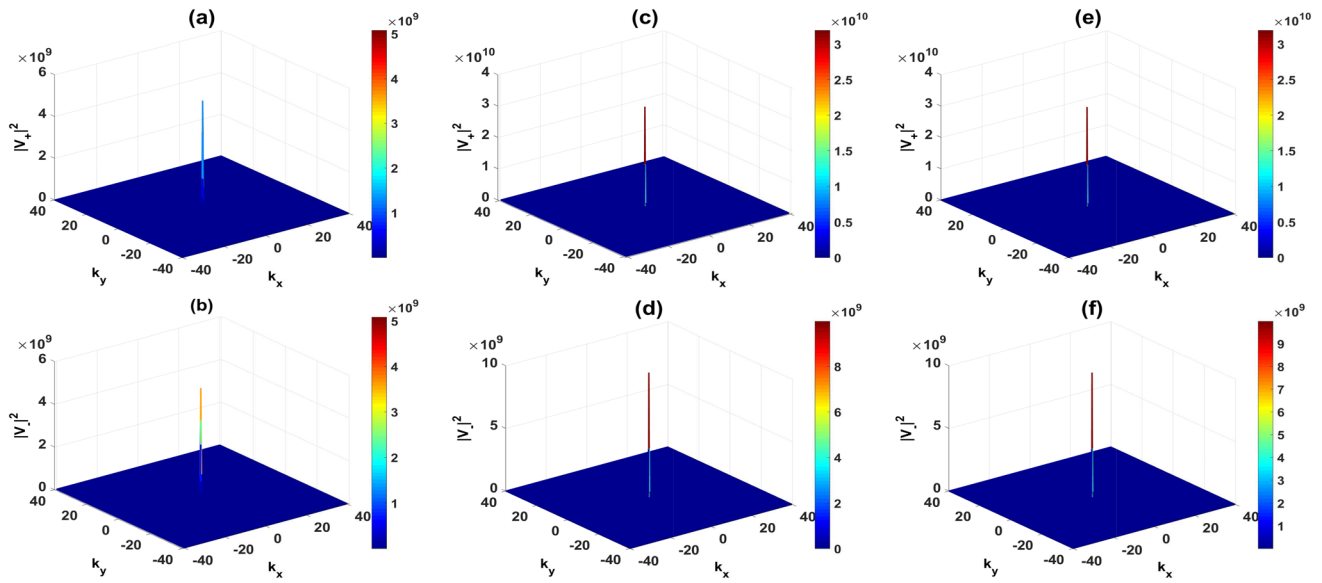
Fig. 9 Spectral profile $|V_+|^2$ (upper line) and $|V_-|^2$ (bottom line) of the results of Fig. 8, at different steps of the evolution: **a, b** $T = 0$, **c, d** $T = 15,000$, **e, f** $T = 30,000$

laser-feedback-based devices, with the capability for sub-wavelength, nanoscale, multidimensional position sensing.

Appendix

A Multimodal method

The equations describing the interaction of the electromagnetic field with the matter are given by the Maxwell–Bloch Eqs. (1a)–(1c). The quantities **E**, **P** and D are taken as follows:

$$\mathbf{E} = \sum_{j=1}^{\infty} \in^{j} \sum_{n=-j}^{+j} \mathbf{E}_{j}^{n}(r) \exp(inwt), \tag{24}$$

$$\mathbf{P} = \sum_{j=1}^{\infty} \in^{j} \sum_{n=-j}^{+j} \mathbf{P}_{j}^{n}(r) \exp(inwt), \tag{25}$$

$$D = \sum_{j=1}^{\infty} \in^{j} \sum_{n=-j}^{+j} D_{j}^{n}(r) \exp(inwt), \tag{26}$$

under the conditions $\mathbf{E}_{j}^{-n} = (\mathbf{E}_{j}^{n})^{*}$, $\mathbf{P}_{j}^{-n} = (\mathbf{P}_{j}^{n})^{*}$, and $D_{j}^{-n} = (D_{j}^{n})^{*}$. We assume that the permanent electric field such that

$$\forall j > 0 \text{ leads to } \mathbf{E}_{j}^{0} = 0. \tag{27}$$

We focus our study to the case $E = E_1^1$, $D_1^0 = D_0$. In the presence of the intense field in the system, we have $D_0 << \frac{2}{\hbar w_a}\left(E \cdot \frac{\partial P}{\partial t}\right)$. Inserting the relation of **P** and D given by Eqs. (25) and (26) into Eqs. (1b) and (1c), it comes, for any $e^{inw_a t}$, the following relations:

$$w_a\left[(1 - n^2)w_a + i\gamma_{\perp}\right](\epsilon P_1^n + \epsilon^2 P_2^n + \epsilon^3 P_3^n + \cdots)$$
$$= -g \sum_{p+q=n} (\epsilon D_1^q + \epsilon^2 D_2^q)(\epsilon E_1^p + \epsilon^2 E_2^p) \tag{28}$$

$$(\gamma_{\parallel} + inw_a)(\epsilon D_1^n + \epsilon^2 D_2^n + \cdots)$$
$$= \frac{2i}{\hbar} \sum_{p+q=n} q(\epsilon E_1^q + \epsilon^2 E_2^q + \cdots)$$
$$\times (\epsilon P_1^q + \epsilon^2 P_2^q + \epsilon^3 P_3^q + \cdots) \tag{29}$$

where p and q can take negative values, and $p + q = n$. For any power of ϵ, solving these equations leads to:

$$\epsilon^1, n = 0: \quad \mathbf{P}_1^0 = 0, \quad D_1^0 = D_0, \tag{30}$$

$$\epsilon^1, n = 1: \quad \mathbf{P}_1^1 = \frac{1}{\mu_0 c^2}\left(-1 + \frac{ik}{w_a}\right)\mathbf{E}_1^1, \quad D_1^1 = 0, \tag{31}$$

$$\epsilon^2, n = 0: \quad \mathbf{P}_2^0 = 0, \quad D_2^0 = \frac{2i}{\hbar\gamma_{\parallel}}\left(\mathbf{P}_1^1 \mathbf{E}_1^{-1} - \mathbf{P}_1^{-1}\mathbf{E}_1^1\right), \tag{32}$$

$$\epsilon^2, n = 1: \quad \mathbf{P}_2^1 = \frac{ig}{\gamma_{\perp} w_a}\left(D_1^0 \mathbf{E}_1^1\right), \quad D_2^1 = 0, \tag{33}$$

$$\epsilon^2, n = 2 : \quad \mathbf{P}_2^2 = 0, \quad D_2^2 = \frac{2i}{\hbar(\gamma_\parallel + 2iw_a)}(\mathbf{P_1^1 E_1^1}), \quad (34)$$

$$\epsilon^3, n = 0 : \quad \mathbf{P}_3^0 = 0, \quad D_3^0 = \frac{2i}{\hbar\gamma_\parallel}(\mathbf{P}_2^1 \mathbf{E}_1^{-1} - \mathbf{P}_2^{-1} \mathbf{E}_1^1), \quad (35)$$

$$\epsilon^3, n = 1 : \quad \mathbf{P}_3^1 = \frac{ig}{\gamma_\perp w_a}(D_2^0 \mathbf{E}_1^1 + D_2^2 \mathbf{E}_1^{-1}), \qquad D_3^1 = 0, \quad (36)$$

$$\epsilon^3, n = 2 : \quad \mathbf{P}_3^2 = 0, \quad D_3^2 = \frac{2i}{\hbar(\gamma_\parallel + 2iw_a)}(\mathbf{P}_2^1 \mathbf{E}_1^1), \quad (37)$$

$$\epsilon^3, n = 3 : \quad \mathbf{P}_3^3 = \frac{ig}{(8w_a - 3i\gamma_\perp)}(D_2^2 \mathbf{E}_1^1), \quad D_3^3 = 0, \quad (38)$$

with $\mathbf{P} = \epsilon \mathbf{P}_1 + \epsilon^2 \mathbf{P}_2 + \epsilon^3 \mathbf{P}_3$
   where $\mathbf{P}_1 = \mathbf{P}_1^1$, $\quad \mathbf{P}_2 = \mathbf{P}_2^1$
   and

$$\mathbf{P}_3 = \mathbf{P}_3^1 + \mathbf{P}_3^3. \quad (39)$$

In the following, we perform the nonlinear perturbation analysis near the laser threshold by introducing a small parameter ϵ so that $D_0 = D_{0C} + \epsilon^2 \tilde{D}_0$ ($\epsilon << 1$), $(\xi, \zeta) = \epsilon(x, y)$, $(Z, \tau) = \epsilon^2(z, t)$ [31]. Moreover,

$$\begin{pmatrix} \mathbf{E} \\ \partial_t \mathbf{E} \\ \mathbf{P} \\ \partial_t \mathbf{P} \\ D \end{pmatrix} = \begin{pmatrix} 0 \\ 0 \\ 0 \\ 0 \\ D_0 \end{pmatrix} + \epsilon \begin{pmatrix} \mathbf{E}_1 \\ \partial_t \mathbf{E}_1 \\ \mathbf{P}_1 \\ \partial_t \mathbf{P}_1 \\ D_1 \end{pmatrix} + \epsilon^2 \begin{pmatrix} \mathbf{E}_2 \\ \partial_t \mathbf{E}_2 \\ \mathbf{P}_2 \\ \partial_t \mathbf{P}_2 \\ D_2 \end{pmatrix} + \quad (40)$$

with

$$\begin{pmatrix} \mathbf{E}_1 \\ \partial_t \mathbf{E}_1 \\ P_1 \\ \partial_t \mathbf{P}_1 \\ D_1 \end{pmatrix} = \begin{pmatrix} A \\ iw_a \mathbf{A} \\ \frac{1}{\mu_0 c^2}(-1 + \frac{ik}{w_a})\mathbf{A} \\ \frac{iw_a}{\mu_0 c^2}(-1 + \frac{ik}{w_a})\mathbf{A} \\ 0 \end{pmatrix} e^{i(wt - k_c z)} + c.c., \quad A \perp \hat{Z}. \quad (41)$$

From the MB equations, some algebraic manipulations yield the following solvability condition

$$\kappa \frac{\partial \mathbf{E}_1}{\partial \tau} = -2iw_a \frac{\partial \mathbf{E}_1}{\partial \tau} - 2iw_a c\left(\frac{\partial}{\partial Z} + \frac{i}{2k_c}\nabla_\perp^2\right)\mathbf{E}_1$$
$$- \mu_0 c^2 \left(2\frac{\partial}{\partial \tau}\frac{\partial \mathbf{P}_1}{\partial t}\right), \quad (42)$$

$$2\frac{\partial}{\partial \tau}\frac{\partial \mathbf{P}_1}{\partial t} = -\gamma_\perp 2\frac{\partial \mathbf{P}_1}{\partial \tau} - g(\tilde{D}_0 + D_2)\mathbf{E}_1, \quad (43)$$

$$\frac{\partial D_2}{\partial t} = -\gamma_\parallel D_2 + \frac{2}{\hbar w_a}\left(\mathbf{E}_1 \cdot \frac{\partial \mathbf{P}_1}{\partial t}\right). \quad (44)$$

D_2 is obtained by solving Eq. (44), and by combining Eqs. (42) and (43) just give

$$\frac{\partial \mathbf{E}_1}{\partial \tau} = \frac{2c(\gamma_\perp - iw_a)}{k - \gamma_\perp + 2iw_a}\left(\frac{\partial}{\partial Z} + \frac{i}{2k_c}\nabla_\perp^2\right)\mathbf{E}_1$$
$$+ \frac{\mu_0 c^2 g}{k - \gamma_\perp + 2iw_a}(\tilde{D}_0 + D_2)\mathbf{E}_1 \quad (45)$$

The nonlinearities come from the interaction between the population inversion and the electric field. To analyze the higher order diffusive term in this system, the higher-order correction $\gamma_\perp^2 \frac{\partial^2 \mathbf{P_1}}{\partial \tau^2}$ is needed to the polarization Eq. (43)

$$\kappa \frac{\partial \mathbf{E}_1}{\partial \tau} = -2iw_a \frac{\partial \mathbf{E}_1}{\partial \tau}$$
$$- 2iw_a c\left(\frac{\partial}{\partial Z} + \frac{i}{2k_c}\nabla_\perp^2\right)\mathbf{E}_1 - \mu_0 c^2 \left(2\frac{\partial}{\partial \tau}\frac{\partial \mathbf{P}_1}{\partial t}\right). \quad (46)$$

$$2\frac{\partial}{\partial \tau}\frac{\partial \mathbf{P}_1}{\partial t} = -\gamma_\perp \frac{\partial \mathbf{P}_1}{\partial t} + \gamma_\perp^2 \frac{\partial^2 \mathbf{P}_1}{\partial \tau^2} - g(\tilde{D}_0 + D_2)\mathbf{E}_1. \quad (47)$$

$$\frac{\partial D_2}{\partial t} = -\gamma_\parallel D_2 + \frac{2}{\hbar w_a}\left(\mathbf{E}_1 \cdot \frac{\partial \mathbf{P}_1}{\partial t}\right). \quad (48)$$

Substituting Eq. (47) into Eq. (46), we obtain

$$(\kappa - \gamma_\perp + 2iw_a)\left[1 + \frac{2\gamma_\perp^2}{\kappa - \gamma_\perp + 2iw_a}\left(\frac{\partial}{\partial Z} + \frac{i}{2k_c}\nabla_\perp^2\right)\right]$$
$$\frac{\partial \mathbf{E}_1}{\partial T} = 2c(\gamma_\perp - iw_a)\left(\frac{\partial}{\partial Z} + \frac{i}{2k_c}\nabla_\perp^2\right)\mathbf{E}_1 + \mu_0 c^2 g(\tilde{D}_0 + D_2)\mathbf{E}_1. \quad (49)$$

Multiplying both sides of Eq. (49) by

$$\left(\left(\kappa - \gamma_\perp + 2iw_a\right)\left[1 + \frac{2\gamma_\perp^2}{\kappa - \gamma_\perp + 2iw_a}\left(\frac{\partial}{\partial Z} + \frac{i}{2k_c}\nabla_\perp^2\right)\right]\right)^{-1}$$

leads to the following amplitude equation derived by Gil [31]:

$$\frac{\partial}{\partial \tau}\mathbf{A} = C_1 A + C_2\left(\frac{\partial}{\partial Z} + \frac{i}{2k_c}\nabla_\perp^2\right)\mathbf{A} + C_3\left(\frac{\partial}{\partial Z} + \frac{i}{2k_c}\nabla_\perp^2\right)^2 \mathbf{A}$$
$$+ C_4(\mathbf{A} \cdot \mathbf{A}^*)\mathbf{A} + C_5(\mathbf{A} \cdot \mathbf{A})\mathbf{A}^*, \quad (50)$$

with

$$C_1 = \frac{\mu_0 c^2 g \tilde{D}_0 (\kappa - \gamma_\perp + 2iw_a)}{} \times ((\kappa - \gamma_\perp)^2 + 4w_a^2), \quad (51)$$

$$C_2 = -\frac{2c\left(\gamma_\perp(\gamma_\perp - \kappa) + 2w_a^2 + iw_a(\kappa - 3\gamma_\perp)\right)}{\times\left((\kappa - \gamma_\perp)^2 + 4w_a^2\right)},$$
(52)

$$C_3 = -\frac{4c^2\gamma_\perp\left(\gamma_\perp^2(2\kappa - \gamma_\perp) + \kappa(\kappa\gamma_\perp - 4w_a^2) - i\gamma_\perp(3\gamma_\perp^2 + 4w_a^2 - \kappa(2\gamma_\perp^2 - \kappa))\right)}{\times\left((\kappa - \gamma_\perp)^2 + 4w_a^2\right)^2},$$
(53)

$$C_4 = \frac{4kg\left(-(\kappa - \gamma_\perp) + 2iw_a\right)}{\times \hbar w_a \gamma_\parallel\left((\kappa - \gamma_\perp)^2 + 4w_a^2\right)},$$
(54)

$$C_5 = \frac{2g\left(\gamma_\parallel\left(2w_a^2 + \kappa(\kappa - \gamma_\parallel^2)\right) - 2w_a^2(\kappa + \gamma_\perp) - iw_a\left(\gamma_\parallel(\kappa + \gamma_\perp) + 2\kappa(\kappa - \gamma_\perp) + 4w_a^2\right)\right)}{\times \hbar w_a\left(\gamma_\parallel^2 + 4w_a^2\right)\left((\kappa - \gamma_\perp)^2 + 4w_a^2\right)}.$$
(55)

$$\frac{\partial D_2}{\partial t} = -\gamma_\parallel D_2 + \frac{2}{\hbar w_a}\left(\mathbf{E_1}.\frac{\partial(\mathbf{P}_1 + \mathbf{P}_3)}{\partial t}\right),$$
(58)

Where D_2 is again obtained by solving Eq. (58), i.e.,

$$D_2 = D_{20} + D_{22}e^{2i(w_a t - k_c z)} + D_{22}^*e^{-2i(w_a t - k_c z)} + D_{24}e^{4i(w_a t - k_c z)} + D_{24}^*e^{-4i(w_a t - k_c z)},$$
(59)

with

$$D_{20} = \frac{4}{\hbar\mu_0 c^2 w_a \gamma_\parallel}\left(-k\mathbf{A}\mathbf{A}^* + \frac{kg\mathbf{A}^2\mathbf{A}^{*2}}{\hbar w_a \gamma_\perp}\left(\frac{4}{\gamma_\parallel} + \frac{1}{(\gamma_\parallel - 2iw_a)} + \frac{1}{(\gamma_\parallel + 2iw_a)}\right)\right.$$
$$\left. + \frac{ig\mathbf{A}^2\mathbf{A}^{*2}}{\hbar w_a \gamma_\perp}\left(\frac{1}{(\gamma_\parallel + 2iw_a)} - \frac{1}{(\gamma_\parallel - 2iw_a)}\right)\right),$$
(60)

To analyze higher order nonlinearities in the system, the nonlinear polarization term $\mathbf{P}_3$ is needed. Therefore, taking into account the nonlinear polarization into the population inversion Eq. (48) yields

$$k\frac{\partial \mathbf{E_1}}{\partial \tau} = -2iw_a\frac{\partial \mathbf{E_1}}{\partial \tau} - 2iw_a c\left(\frac{\partial}{\partial Z} + \frac{i}{2k_c}\nabla_\perp^2\right)\mathbf{E_1} - \mu_0 c^2\left(2\frac{\partial}{\partial \tau}\frac{\partial \mathbf{P}_1}{\partial t}\right),$$
(56)

$$2\frac{\partial}{\partial \tau}\frac{\partial \mathbf{P}_1}{\partial t} = -\gamma_\perp\frac{\partial \mathbf{P}_1}{\partial \tau} + \gamma_\perp^2\frac{\partial^2 \mathbf{P}_1}{\partial T^2} - g(\tilde{D}_0 + D_2)\mathbf{E_1},$$
(57)

$$D_{22} = \frac{2}{\hbar\mu_0 c^2 w_a(\gamma_\parallel + 2iw_a)}\left(-\mathbf{A}^2(k + iw_a)\right.$$
$$+ \frac{2g\mathbf{A}^3\mathbf{A}^*}{\hbar}\left(\frac{k}{\gamma_\perp w_a}\left(\frac{1}{(\gamma_\parallel 2iw_a)} + \frac{2}{\gamma_\parallel}\right)\right.$$
$$+ \frac{3}{(\gamma_\parallel + 2iw_a)(8w_a - 3i\gamma_\perp)}$$
$$\left.\left.+ \frac{i}{(\gamma_\parallel + 2iw_a)}\left(\frac{1}{\gamma_\perp} - \frac{3k}{w_a(8w_a - 3i\gamma_\perp)}\right)\right)\right),$$
(61)

$$D_{24} = \frac{12g\mathbf{A}^4}{\hbar^2\mu_0 c^2 w_a(\gamma_\parallel + 4iw_a)(8w_a - 3i\gamma_\perp)}\left(1 - \frac{ik}{w_a}\right).$$
(62)

Substituting Eq. (59) into Eq. (57), and after some algebra, we obtain the following (3+1)D vectorial cubic-quintic CGL equation

$$\frac{\partial \mathbf{A}}{\partial \tau} = z_1\mathbf{A} + z_2\left(\frac{\partial}{\partial Z} + \frac{i}{2k_c}\nabla_\perp^2\right)\mathbf{A} + z_3\left(\frac{\partial}{\partial Z} + \frac{i}{2k_c}\nabla_\perp^2\right)^2\mathbf{A} + z_4(\mathbf{A}\cdot\mathbf{A}^*)\mathbf{A}$$
$$+ z_5(\mathbf{A}\cdot\mathbf{A})\mathbf{A}^* + z_6(\mathbf{A}^2\cdot\mathbf{A}^{*2})\mathbf{A} + z_7(\mathbf{A}^3\cdot\mathbf{A}^*)\mathbf{A}^*,$$
(63)

with

$$z_1 = \frac{\mu_0 c^2 g \tilde{D}_0 (k - \gamma_\perp + 2iw_a)}{(k - \gamma_\perp)^2 + 4w_a^2}, \tag{64}$$

$$z_2 = \frac{2c(2w_a^2 + \gamma_\perp(\gamma_\perp - k) + iw_a(k - 3\gamma_\perp))}{(k - \gamma_\perp)^2 + 4w_a^2}, \tag{65}$$

$$z_3 = \frac{4c^2 \gamma_\perp \begin{pmatrix} \gamma_\perp^2(2\kappa - \gamma_\perp) + \kappa(\kappa\gamma_\perp - 4w_a^2) \\ -i\gamma_\perp(3\gamma_\perp^2 + 4w_a^2 - \kappa(2\gamma_\perp - \kappa)) \end{pmatrix}}{(\kappa - \gamma_\perp)^2 + w_a^2}, \tag{66}$$

$$z_4 = \frac{4kg((k - \gamma_\perp) - 2iw_a)}{\hbar w_a \gamma_\parallel ((k - \gamma_\perp)^2 + 4w_a^2)}, \tag{67}$$

$$z_5 = \frac{2g \begin{pmatrix} \gamma_\parallel(\kappa(\kappa - \gamma_\perp^2) + 2w_a^2) - 2w_a^2(\kappa + \gamma_\perp) \\ -iw_a(\gamma_\parallel(\kappa + \gamma_\perp) + \kappa(\kappa - \gamma_\perp) + 42w_a^2) \end{pmatrix}}{\hbar w_a((\kappa - \gamma_\perp)^2 + w_a^2)(\gamma_\parallel^2 + 4w_a^2)}, \tag{68}$$

$$z_6 = \frac{8kg^2(\gamma_\parallel(k + 2\gamma_\parallel) + 10w_a^2)(k - \gamma_\perp - 2iw_a)}{\hbar^2 w_a^2 \gamma_\perp \gamma_\parallel^2 ((k - \gamma_\perp)^2 + 4w_a^2)(\gamma_\parallel^2 + 4w_a^2)}, \tag{69}$$

$$z_{7r} = \frac{4g^2 \begin{pmatrix} (\gamma_\parallel(k(3\gamma_\parallel^2 + 4w_a^2) + 4w_a^2\gamma_\parallel)(9\gamma_\perp^2 + 64w_a^2) + 3\gamma_\perp\gamma_\parallel((8w_a^2 \\ + 3k\gamma_\perp)(\gamma_\parallel^2 - 4w_a^2) + 4\gamma_\parallel w_a^2(-8k + 3\gamma_\perp)))(k - \gamma_\perp) \\ + 2w_a^2(((\gamma_\parallel^2 - 4w_a^2 - 4k\gamma_\parallel)\gamma_\parallel - 4k(\gamma_\parallel^2 + 4w_a^2))(9\gamma_\perp^2 + 64w_a^2) \\ + 3\gamma_\parallel\gamma_\perp((-8k + 3\gamma_\perp)(\gamma_\parallel^2 - 4w_a^2) - 4(8w_a^2 + 3k\gamma_\perp)\gamma_\parallel)) \end{pmatrix}}{\hbar^2 w_a^2 \gamma_\perp \gamma_\parallel (\gamma_\parallel^2 + 4w_a^2)^2 (9\gamma_\perp^2 + 64w_a^2)((k - \gamma_\perp)^2 + 4w_a^2)} \tag{70}$$

$$z_{7i} = \frac{4g^2 \begin{pmatrix} (w_a(((\gamma_\parallel^2 - 4(w_a^2 + k\gamma_\parallel)) - 4k(\gamma_\parallel^2 + 4w_a^2))(9\gamma_\perp^2 + 64w_a^2) \\ + 3\gamma_\parallel\gamma_\perp((-8k + 3\gamma_\perp)(\gamma_\parallel^2 - 4w_a^2) - 4\gamma_\parallel(8w_a^2 + 3k\gamma_\parallel)))(k - \gamma_\perp \\ ) - 2(\gamma_\parallel(k(3\gamma_\parallel^2 + 4w_a^2) + 4w_a^2\gamma_\parallel)(9\gamma_\perp^2 + 64w_a^2) + 3w_a\gamma_\parallel\gamma_\perp((8w_a^2 \\ + 3k\gamma_\perp)(\gamma_\parallel^2 - 4w_a^2) + 4w_a^2\gamma_\parallel(3\gamma_\perp - 8k))) \end{pmatrix}}{\hbar^2 w_a^2 \gamma_\perp \gamma_\parallel (\gamma_\parallel^2 + 4w_a^2)^2 (9\gamma_\perp^2 + 64w_a^2)((k - \gamma_\perp)^2 + 4w_a^2)} \tag{71}$$

B Effective potential

The expression of the effective potential derived in Sec. 4 is as follows:

$$U = \left(\frac{32X_0^4}{81X^2} + \frac{1}{X^2} - \frac{28X_0^2}{81} + \frac{4X_0^2}{9X^2} - \frac{13}{36} + \frac{3}{128X_0^2}\right)$$
$$A^8 \delta_i^2 e^{-\frac{16X_0^2}{X^2}} + \left(\frac{8X_0^4}{X^2}\right.$$
$$+ \frac{1}{4X^2} + \left(\frac{17}{18X^2} - \frac{79}{126}\right)X_0^2 - \frac{5X^2}{4} - \frac{53}{84} - \frac{9}{56X_0^2}\right)$$
$$A^6 \delta_i \gamma_i e^{-\frac{14X_0^2}{3X^2}}$$
$$+ ((-\frac{1}{8}(7X^2 + \frac{15}{8X_0^2})\delta_i^2 - \frac{1}{9}(1 + 8X^2 + \frac{16}{9}X_0^2)\delta_i\mu)$$
$$A^8 - (1 + 2X_0^2$$
$$+ 7X^2)A^6\varepsilon\delta_i + (\frac{8}{9}(4C + \frac{\beta}{X^2} - 4\beta\delta_i C^2 X^2)X_0^2\delta_i - \frac{16}{9}(1$$
$$+ 5\beta CX^2)\delta_i NX_0^2 - \frac{8\beta\delta_r CX^2}{3}$$
$$+ 2\beta\delta_i C^2 X^2(X^2 - 1) + 2\delta_i C$$
$$- \frac{4}{3}\delta_r + 2\delta_i CX^2 + \delta_i\beta N^2 X^2 - \delta\delta_i X^2$$
$$+ \frac{\beta\delta_i}{2X^2} - \frac{11}{6}\beta\delta_i - \frac{\delta_i N}{X_0}$$
$$- \frac{3\beta\delta_i}{4X_0^2}A^4)e^{-\frac{8X_0^2}{X^2}}$$
$$+ (-(1 + 2X_0^2 - \frac{11}{2}X^2)\mu\gamma_i A^6 - (1 + 4X^2$$
$$+ 2X_0^2)A^4 + (-\gamma_r - \frac{3}{2}\gamma_i\beta + 2\gamma_i C$$
$$+ 4\gamma_i CX_0^2 - 2\gamma_i NX_0 + 2\beta\gamma_i C^2 X^4$$
$$- \frac{\gamma_i N}{X_p} - \frac{\gamma_i\beta}{2X_0^2} + \frac{\beta\gamma_i}{2X^2} + \frac{\gamma_i\beta X_0^2}{X^2})A^2$$
$$- (\frac{\gamma_i\delta}{2} + 8\beta\gamma_i CX_0 N + 2\beta\gamma_i C^2$$
$$+ \beta\gamma_r C + 4\beta\gamma_i C^2 X_0^2 - \frac{\beta\gamma_i N}{2}))e^{-\frac{2X_0^2}{X^2}} + (\frac{\gamma_i^2 X_0^2}{2X^2}$$
$$+ \frac{\gamma_i^2}{8X^2} - \frac{\gamma_i^2}{4}$$
$$- \frac{3}{32}\gamma_i^2 X^2 - \frac{\gamma_i^2}{16X_0^2} - \frac{\gamma_i^2 X_0^2}{4}$$
$$+ \frac{\gamma_i^2 X_0^2}{2X^2})e^{-\frac{4X_0^2}{X^2}} - \frac{2\mu^2 X^2 A^8}{9} - \frac{5\mu\varepsilon X^2 A^6}{12}$$
$$+ 4\beta^2 C^2 X^2(2C^2 X^4 + 3) - \frac{2}{X^2} + \frac{\beta^2}{2X^2}$$
$$- 8\beta C^3 X^4 - 24\beta C \ln(X)$$
$$+ (\frac{X^2\varepsilon}{4}(\beta N^2 - \delta)$$
$$+ \beta CX^2(-1 + \varepsilon CX^2) + (1 + \beta\varepsilon)\ln(X))A^2$$

References

1. F.T. Arecchi, S. Boccaletti, P.L. Ramazza, Pattern formation and competition. Phys. Rep. **318**, 1–83 (1999)
2. J.R. Tredicce, F.T. Arecchi, G.L. Lippi, G.P. Puccioni, Instabilities in lasers with an injected signal. J. Opt. Soc. Am. B **2**, 173–183 (1985)
3. S. Ciuchi, F. de Pasquale, M. San Miguel, N.B. Abraham, Phase and amplitude correlations induced by the switch-on chirp of a detuned laser. Phys. Rev. A **44**, 7657–7668 (1991)
4. E. Hernandez-Garcia, R. Toral, M.S. Miguel, Intensity correlation functions for the colored gain-noise model of dye lasers. Phys. Rev. A **42**, 6823–6830 (1990)
5. G.P. Agrawal, N.K. Dutta, *Long-Wavelength Semiconductor Lasers* (Van Nostrand 426 Reinhold, New York, 1986)
6. C.O. Weiss, R. Vilaseca, *Dynamics of Lasers* (VCH Publishers, Weinheim, 1991)
7. F. Strumia, in *Advances in Laser Spectroscopy*, ed. by F.T. Arecchi, F. Strumia, H. Walther (Plenum Press, New York, 1983), p. 267
8. P. Colet, R. Roy, Digital communication with synchronized chaotic lasers. J. Opt. Lett. **19**, 2056–2058 (1994)
9. L. Lugiato, F. Prati, M. Brambilla, *Nonlinear Optical Systems* (Cambridge University Press, Cambridge, 2015)
10. W.E. Lamb Jr., Theory of an optical maser. Phys. Rev. **134**, A1429–A1450 (1964)
11. H. Haken, *Laser Theory* (Springer, Berlin, 1984)
12. I. Leyva, J.M. Guerra, Time-resolved pattern evolution in a large-aperture class A laser. Phys. Rev. A **66**, 023820 (2002)
13. F. Encinas-Sanz, I. Leyva, J.M. Guerra, Time resolved pattern evolution in a large aperture laser. Phys. Rev. Lett. **84**, 883–886 (2000)
14. M. Riley, T.D. Padrick, R. Palmer, Multilevel paraxial Maxwell–Bloch equation description of short pulse amplification in the atomic iodine laser. IEEE J. Quantum Electron. QE **15**, 178–189 (1979)
15. P. Coullet, L. Gil, F. Rocca, Optical vortices. Opt. Commun. **73**, 403–408 (1989)
16. K. Staliunas, C.O. Weiss, Tilted and standing waves and vortex lattices in class-A lasers. Phys. D **81**, 79–93 (1995)
17. S.C. Mancas, S.R. Choudhury, Traveling wavetrains in the complex cubicquintic Ginzburg–Landau equation. Chaos Solitons Fractals **28**, 834–843 (2006)
18. S. Liu, S. Liu, Z. Fu, Q. Zhao, The Hopf bifurcation and spiral wave solution of the complex Ginzburg–Landau equation. Chaos Solitons Fractals **13**, 1377–1381 (2002)
19. M. Jun, G. Ji-Hua, W. Chun-Ni, S. Jun-Yan, Control spiral and multi-spiral wave in the complex Ginburg–Landau equation. Chaos Solitons Fractals **38**, 521–530 (2008)
20. K. Staliunas, Laser Ginzburg–Landau equation and laser hydrodynamics. Phys. Rev. A **48**, 1573–1581 (1993)
21. G.L. Oppo, G. D'Alessandro, W.J. Firth, Spatiotemporal instabilities of lasers in models reduced via center manifold techniques. Phys. Rev. A **44**, 4712–4720 (1991)
22. J.M. Soto-Crespo, N.N. Akhmediev, V.V. Afanasjev, Stability of the pulselike solutions of the quintic complex Ginzburg–Landau equation. J. Opt. Soc. Am. B **13**, 1439–1449 (1996)
23. J. Lega, J.V. Moloney, A.C. Newell, Swift–Hohenberg equation for lasers. Phys. Rev. Lett. **73**, 2978–2981 (1994)
24. M. Tlidi, M. Giorgiou, P. Mandel, Transverse patterns in nascent optical bistability. Phys. Rev. A **48**, 4605–4609 (1993)
25. H.A. Haus, A. Mecozzi, Noise of mode-locked lasers. IEEE J. Quantum Electron. **29**, 983–996 (1993)
26. C.R. Menyuk, J.K. Wahlstrand, J. Willits, R.P. Smith, T.R. Schibli, S.T. Cundiff, Pulse dynamics in mode-locked lasers: relaxation oscillations and frequency pulling. Opt. Express **15**, 6677–6689 (2007)
27. W.W. Hsiang, C.Y. Lin, Y. Lai, Stable new bound soliton pairs in a 10 GHz hybrid frequency modulation mode-locked Er-fiber laser. Opt. Lett. **31**, 1627–1629 (2006)
28. W. Chang, N. Akhmediev, S. Wabnitz, Effect of an external periodic potential on pairs of dissipative solitons. Phys. Rev. A **80**, 013815 (2009)
29. J.N. Kutz, Mode-locked soliton lasers. SIAM Rev. **48**, 629–678 (2006)
30. J.M. Soto-Crespo, N. Akhmediev, A. Ankiewicz, Pulsating, creeping, and erupting solitons in dissipative systems. Phys. Rev. Lett. **85**, 2937–2940 (2000)
31. L. Gil, Vector order parameter for an unpolarized laser and its vectorial topological defects. Phys. Rev. Lett. **70**, 162–165 (1993)
32. A. Amengual, E. Hernandez-Garcia, R. Montagne, M. San Miguel, Synchronization of spatiotemporal chaos: the regime of coupled spatiotemporal intermittency. Phys. Rev. Lett. **78**, 4379–4382 (1997)
33. E. Hernandez-Garcia, M. Hoyuelos, P. Colet, M. San Miguel, R. Montagne, Spatiotemporal chaos, localized structures and synchronization in the vector complex Ginzburg–Landau equation. Int. J. Bifurc. Chaos **9**, 2257–2264 (1999)
34. M. Hoyuelos, E. Hernandez-Garcia, P. Colet, M.S. Miguel, Defect-freezing and defect-unbinding in the vector complex Ginzburg–Landau equation. Comput. Phys. Comm. **121**, 414–419 (1999)
35. E. Hernandez-Garcia, M. Hoyuelos, P. Colet, M.S. Miguel, Dynamics of localized structures in vectorial waves. Phys. Rev. Lett. **85**, 744–747 (2000)
36. M. Hoyuelos, E. Hernandez-Garcia, P. Colet, M.S. Miguel, Dynamics of defects in the vector complex Ginzburg–Landau equation. Phys. D **174**, 176–197 (2003)
37. W.-L. Zhu, Y.-J. He, Stability conditions for moving dissipative solitons in one- and multidimensional systems with a linear potential. Opt. Express **18**, 17053–17058 (2010)
38. M. Djoko, T.C. Kofane, Dissipative optical bullets modeled by the cubic-quintic-septic complex Ginzburg–Landau equation with higher-order dispersions. Commun. Nonlinear Sci Numer. Simul. **48**, 179–199 (2017)
39. M. Djoko, C.B. Tabi, T.C. Kofane, Effects of the septic nonlinearity and the initial value of the radius of orbital angular momentum beams on data transmission in optical fibers using the cubic-quintic-septic complex Ginzburg–Landau equation in presence of higher-order dispersions. Chaos Solitons Fractals **147**, 110957 (2021)
40. D. Mihalache, D. Mazilu, L.C. Crasovan, L. Torner, B.A. Malomed, F. Lederer, Three-dimensional walking spatiotemporal solitons in quadratic media. Phys. Rev. E **62**, 7340–7347 (2000)
41. B.A. Malomed, Multidimensional solitons: well-established results and novel findings. Eur. Phys. J. Spec. Top. **225**, 2507–2532 (2016)
42. Y.V. Kartashov, G.E. Astrakharchik, B.A. Malomed, L. Torner, Frontiers in multidimensional self-trapping of nonlinear fields and matter. Nat. Rev. Phys. **1**, 185–197 (2019)
43. D. Mihalache, Localized structures in optical and matter-wave media: a selection of recent studies. Rom. Rep. Phys. **73**, 403 (2021)

44. A. Djazet, C.B. Tabi, S.I. Fewo, T.C. Kofane, Vector dissipative light bullets in optical laser beam. Appl. Phys. B **126**, 74 (2020)

45. A.E. Siegman, Lasers (University Science Books, Mill Valley, 1986), p. 943, Eq. (50) and p. 946, Eq. (56)

46. R.W. Boyd, *Nonlinear Optics-Second Edition* (Academic Press, New York, 2003)

47. A. Djazet, S.I. Fewo, C.B. Tabi, T.C. Kofane, On a laser (3+1)-dimensional vectorial cubic-quintic complex Ginzburg–Landau equation and modulational instability (2019). https://doi.org/10.20944/preprints201910.0171.v1

48. L.A. Lugiato, G.L. Oppo, J.R. Tredicce, L.M. Narducci, M.A. Pernigo, Instabilities and spatial complexity in a laser. J. Opt. Soc. Am. B **7**, 1019–1033 (1990)

49. M. Hoyuelos, E. Hernandez-Garcia, P. Colet, M.S. Miguel, Dynamics of defects in the vector complex Ginzburg–Landau equation. Phys. D **174**, 176–197 (2003)

50. Y. Kuramoto, in *Chemical Oscillations, Waves and Turbulence*, ed. by H. Haken. Springer Series in Synergetics, vol. 19 (Springer, Berlin, 1984)

51. V. Skarka, N.B. Aleksic, H. Leblond, B.A. Malomed, D. Mihalache, Varieties of stable vortical solitons in Ginzburg–Landau media with radially inhomogeneous losses. Phys. Rev. Lett. **105**, 213901 (2010)

52. V. Skarka, N.B. Aleksic, M. Lekic, B.N. Aleksic, B.A. Malomed, D. Mihalache, H. Leblond, Formation of complex two-dimensional dissipative solitons via spontaneous symmetry breaking. Phys. Rev. A **90**, 023845 (2014)

53. M.D. Mboumba, A.B. Moubissi, T.B. Ekogo, G.H. Ben-Bolie, T.C. Kofane, Variational approach for two-component condensates dynamics with two-and three-body interactions and external feeding. Int. J. Mod. Phys. B **29**, 1550202 (2015)

54. S.I. Fewo, C.M. Ngabireng, T.C. Kofane, Ultrashort optical solitons in the cubic-quintic complex Ginzburg–Landau equation with higher-order terms. J. Phys. Soc. **7**, 074401 (2008)

55. M. Djoko, T.C. Kofane, The cubic-quintic-septic complex Ginzburg–Landau equation formulation of optical pulse propagation in 3D doped Kerr media with higher-order dispersions. Opt. Commun. **416**, 190–201 (2018)

56. Y. Qiu, B.A. Malomed, D. Mihalache, X. Zhu, L. Zhang, Y. He, Soliton dynamics in a fractional complex Ginzburg–Landau model. Chaos Solitons Fractals **131**, 109471 (2020)

57. V. Skarka, D.V. Timotijevic, N.B. Aleksic, Extension of the stability criterion for dissipative optical soliton solutions of a two-dimensional Ginzburg–Landau system generated from asymmetric inputs. J. Opt. A Pure Appl. Opt. **10**, 075102 (2008)

58. V. Skarka, V.I. Berezhehiani, R. Miklaszewski, Spatiotemporal soliton propagation in saturating nonlinear optical media. Phys. Rev. E. **56**, 1080–1087 (1997)

59. N. Akhmediev, J.M. Soto-Crespo, G. Town, Pulsating solitons, chaotic solitons, period doubling, and pulse coexistence in model-locked laser: complex Ginzburg–Landau equation approach. Phys. Rev. E **63**, 05602 (2001)

60. L.-C. Crasovan, B.A. Malomed, D. Mihalache, Stable vortex solitons in the two-dimensional Ginzburg–Landau equation. Phys. Rev. E **63**, 016605 (2001)

61. F. Encinas-Sanz, S. Melle, O.G. Calderon, Time-resolved dynamics of two-dimensional transverse patterns in broad area lasers. Phys. Rev. Lett. **93**, 213904 (2004)

62. J. Ohtsubo, Semiconductor Lasers Stability, Instability and Chaos. Springer in Optical Sciences, vol. 111 (2013)

63. K.J. Kuhn, *Laser Engineering* (Prentice Hall, Hoboken, 1998)

64. H. Kapteyn, O. Cohen, I. Christov, M. Murnane, Harnessing attosecond science in the quest for coherent X-rays. Science **317**, 775–778 (2007)

65. S.D. Cohen, A. Aragoneses, D. Rontani, M.C. Torrent, C. Masoller, D.J. Gauthier, Multidimensional subwavelength position sensing using a semiconductor laser with optical feedback. Opt. Lett. **38**, 4331–4334 (2013)

66. D. Dangoisse, D. Hennequin, C. Lepers, E. Louvergneaux, P. Gloriex, Two-dimensional optical lattices in a laser. Phys. Rev. A **46**, 5955–5958 (1992)